A reduced basis model with parametric coupling for fluid-structure interaction problems

Toni Lassila, Alfio Quarteroni, Gianluigi Rozza

A reduced basis model with parametric coupling for fluid-structure interaction problems

Toni Lassila[♯,§], Alfio Quarteroni[§,†] and Gianluigi Rozza[§]

January 10, 2011

[♯] Institute of Mathematics and Systems Analysis, Aalto University, Helsinki, Finland.
[§] Modeling and Scientific Computing, MATHICSE-CMCS, École Polytechnique Fédérale de Lausanne, EPFL, Station 8, CH-1015 Lausanne, Switzerland.
[†] MOX– Modellistica e Calcolo Scientifico, Dipartimento di Matematica "F. Brioschi" Politecnico di Milano, via Bonardi 9, 20133 Milano, Italy

Abstract

We present a new model reduction technique for steady fluid-structure interaction problems. When the fluid domain deformation is suitably parametrized, the coupling conditions between the fluid and structure can be formulated in the low-dimensional space of geometric parameters. Moreover, we apply the reduced basis method to reduce the cost of repeated fluid solutions necessary to achieve convergence of fluid-structure iterations. In this way a reduced order model with reliable a posteriori error bounds is obtained. The proposed method is validated with an example of steady Stokes flow in an axisymmetric channel, where the structure is described by a simple 1-d generalized string model. We demonstrate rapid convergence of the reduced solution of the parametrically coupled problem as the number of geometric parameters is increased.

1 Introduction

The numerical simulation of Fluid-Structure Interaction (FSI) problems is an important topic in wide areas of engineering and medical research. Concerning the latter, of great importance is the modelling of blood flow in the large arteries of the human cardiovascular system, where pulsatile flows combined with a high degree of deformability of the arterial walls together cause

large displacement effects that cannot be neglected when attempting to accurately model the flow dynamics of the system. High fidelity computational fluid dynamics and structural mechanics solvers based on, for example, the Finite Element Method (FEM) need to be combined in a framework that is challenging both from a mathematical as well as implementation viewpoint. For an overview of cardiovascular modelling techniques we refer to [40, 42] and the book [13]. The complexity and nonlinearity of FSI problems has until recently limited the scope of physically meaningful simulations to just small and isolated sections of arteries. When attempting to consider the entire cardiovascular system as a complex network of different time and spatial scales, Model Order Reduction (MOR) techniques can accurately and reliably reduce the nonlinear FSI models to computationally more cost-efficient ones.

In the geometric multiscale approach to MOR [12] the flow network is decomposed to smaller parts that are joined together using physical coupling conditions, and each part of which is modelled at a level necessary to capture the relevant local dynamics of the system. The target for our proposed reduced model is those parts of the cardiovascular network, where a full fidelity 3-d Navier-Stokes solution is not necessary, but where fluid-structure interaction effects are still important. The reduced model should fulfill two conditions: (i) it should have certified a posteriori error bounds that can be tuned to the user's requirements, and (ii) it should have sufficiently low online computational memory requirements to fit on one parallel node of a supercomputer.

An important aspect of any large-displacement FSI problem is finding the configuration of the interface between fluid and structure. The process is typically iterative: a trial configuration of the geometry is used to solve the fluid and structure subproblems, the coupling conditions are tested, and if they are not satisfied within a desired degree of accuracy then the trial configuration is updated and the step is repeated. A traditional approach to FSI is that the discrete mesh is updated on each iteration by moving the boundary nodes and adjusting the interior mesh points to ensure mesh quality. This approach leads to a large number of coupling variables (the total number of mesh points on the free boundary). An external parametrization of the geometry can be used to drive down the number of coupling variables. When considering simple flow geometries the shape of the deformable wall can be directly parametrized e.g. with splines. For realistic geometries it might be necessary to parametrize the geometry in a way that is relatively independent of its description.

There are many shape parametrization methods to choose from. Comparisons of different shape parametrization techniques from a fluid dynamics viewpoint can be found in [51], and from a model reduction viewpoint in [49]. We propose to describe the deformations of the fluid channel with Free-Form Deformations (FFDs) [52]. They are a technique for smooth parametric de-

formations of arbitrary shapes embedded in the grid of control points. FFDs can be used to give a flexible and global parametric deformation of a fixed reference domain that is completely independent of the shape and its computational mesh. Model reduction for FFD-based shape parametrizations has been previously considered for the shape design of airfoils in potential [26] and thermal flows [48]. In cardiovascular applications, FFDs have been used to track the motion of the left ventricle (see [32] for a review), and to solve an optimal shape design problem of an aorto-coronaric bypass anastomoses [31].

After parametrizing the geometry with a FFDs we need to address the coupling between fluid and structure. We use the deformation parameters of the FFD as coupling variables. A fixed point coupling algorithm can be written in the parameter space rather than the displacement space. Again an iterative procedure is needed to ensure the coupling conditions are satisfied to a desired tolerance. Thus a potentially large number of parametric PDE solutions for the fluid equations need to be performed in different parametric configurations.

To reduce the memory requirements and the online computational cost of solving the fluid system, we apply the Reduced Basis (RB) method (originally proposed and analyzed in [1, 10, 35, 39]). It is a reliable MOR method for parametric PDEs. An overview can be found in [47] and a more detailed exposition in [36]. The attractiveness of these methods is based on their ability to give certified a posteriori bounds on the error of the field solutions and their outputs when compared to the underlying FEM solution. We use the reduced basis method to reduce the computational cost of the steady Stokes equations in different configurations of the geometry.

The structure is the following: in Sect. 2 we introduce the steady FSI problem of incompressible Stokes equations coupled to an elliptic 1-d generalized string equation. This is a benchmark problem for which the existence of solutions has been demonstrated in [17, 18] and whose numerical solution has been previously considered e.g. in [28, 33, 53]. In Sect. 3 we discuss the geometric parametrization and introduce the free-form deformations. In Sect. 4 we couple the fluid and structure in the space of parametric deformations. In Sect. 5 the reduced basis method for the fluid equations is detailed, and we discuss a posteriori error bounds of the solutions. In Sect. 6 we present numerical results validating our approach. Sect. 7 contains some conclusions.

2   The steady fluid-structure interaction model

We use the following standard notations: $\Omega \subset \mathbb{R}^d$, $d = 1, 2, 3$, is a bounded open set, $H^k(\Omega)$ is the Sobolev space of functions with weak derivatives up to order k square-integrable on X, $H^{k-1/2}(\partial\Omega)$ is the space of functions

3

that are traces of $H^k(\Omega)$ on the boundary $\partial\Omega$, $H_0^k(\Omega)$ is the subspace of functions whose trace vanishes on $\partial\Omega$; $C^{k,\alpha}(\Omega)$ is the space of functions with derivatives up to order k being Hölder-continuous with exponent $0 < \alpha \leq 1$ (if $\alpha = 1$ these are the Lipschitz-continuous functions); $L^2(\Omega)$ is the space of square-integrable functions, and $L^\infty(\Omega)$ is the space of essentially bounded functions on Ω.

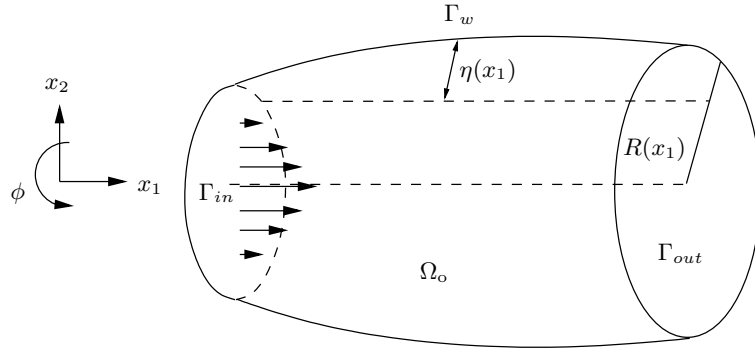## 2.1 Fluid model: the steady incompressible Stokes equations

Figure 1: Axisymmetric flow geometry for the fluid-structure interaction model problem

We assume the flow geometry represented in Fig. 1 that is axisymmetric with cylindrical coordinates $(\boldsymbol{x}, \phi) = (x_1, x_2, \phi) \in \Omega_{\mathrm{o}} \times [0, 2\pi)$. The lengthwise cross-section of the domain $\Omega_{\mathrm{o}} := (0, L) \times (0, R)$ depends on the unknown radius $R(x_1)$ of the channel, which satisfies $R(x_1) := R_0 + \eta(x_1) > 0$, where $\eta \in H_0^2(0, L)$ is a function describing the smooth displacement of the outer wall from its reference configuration (a cylindrical tube of radius $R_0 > 0$). We assume also axisymmetric forces, $\boldsymbol{f} = \boldsymbol{f}(\boldsymbol{x})$ and $\boldsymbol{g} = \boldsymbol{g}(x_2)$. Owing to the axial symmetry we can consider the steady Stokes equations for incompressible fluid flow in the two-dimensional domain $\Omega_o(\eta)$ with mixed boundary conditions on its boundary $\Gamma(\eta) = \Gamma_{in} \cup \Gamma_{out} \cup \Gamma_w(\eta)$, that is

$$
\begin{cases}
\nabla \cdot \boldsymbol{\sigma} + \boldsymbol{f} = 0 & \text{in } \Omega_{\mathrm{o}}(\eta) \\
\nabla \cdot \boldsymbol{u} = 0 & \text{in } \Omega_{\mathrm{o}}(\eta) \,, \qquad (2.1) \\
\boldsymbol{u} = \boldsymbol{0} \text{ on } \Gamma_w, \quad \boldsymbol{u} = \boldsymbol{g} \text{ on } \Gamma_{in}, \quad \boldsymbol{\sigma} \cdot \boldsymbol{n} = \boldsymbol{0} & \text{on } \Gamma_{out}
\end{cases}
$$

where $\boldsymbol{u}$ is the fluid velocity field, and $\boldsymbol{\sigma}$ is the symmetric Cauchy stress tensor. The data are assumed to have the following regularity: $\boldsymbol{f} \in [L^2(\Omega_{\mathrm{o}})]^2$ and $\boldsymbol{g} \in H^{1/2}(\Gamma)$, where the space $[H^{1/2}(\Gamma)]^2 = \boldsymbol{\gamma}_\Gamma([H^1(\Omega_{\mathrm{o}})]^2)$ is defined as usual with the continuous trace operator $\boldsymbol{\gamma}_\Gamma$ on Γ. We denote by $\widehat{\boldsymbol{g}} \in [H_0^1(\Omega_{\mathrm{o}})]^2$ any continuous extension of the Dirichlet data to the fluid domain. Assuming a Newtonian fluid, the stress-strain relationship is given

4

by $\boldsymbol{\sigma} = -p\boldsymbol{I} + \nu \left(\nabla \boldsymbol{u} + \nabla \boldsymbol{u}^t \right)$, where ν denotes the dynamic viscosity and p is the pressure field. After choosing the velocity space $\mathcal{V} := [H^1_{\Gamma_d}(\Omega_{\mathrm{o}}(\eta))]^2$ of functions that vanish on $\Gamma_d = \Gamma_{in} \cup \Gamma_w$ and the pressure space $\mathcal{Q} := L^2(\Omega_{\mathrm{o}}(\eta))$, a mixed weak formulation of the equations is to find $\boldsymbol{u} \in \mathcal{V}$ and $p \in \mathcal{Q}$ s.t.

$$\begin{cases} \displaystyle\int_{\Omega_{\mathrm{o}}} [\nu \nabla \boldsymbol{u} : \nabla \boldsymbol{v} - p \nabla \cdot \boldsymbol{v}] \, d\Omega = \int_{\Omega_{\mathrm{o}}} \boldsymbol{f} \cdot \boldsymbol{v} \, d\Omega - \int_{\Omega_{\mathrm{o}}} \nu \nabla \widehat{\boldsymbol{g}} \cdot \nabla \boldsymbol{v} \, d\Omega & \text{for all } \boldsymbol{v} \in \mathcal{V} \\ \displaystyle -\int_{\Omega_{\mathrm{o}}} q \nabla \cdot \boldsymbol{u} \, d\Omega = \int_{\Omega_{\mathrm{o}}} q \nabla \cdot \widehat{\boldsymbol{g}} \, d\Omega & \text{for all } q \in \mathcal{Q} \end{cases}.$$
$$(2.2)$$

For notational brevity we define the bilinear forms

$$\mathcal{A}(\boldsymbol{u}, \boldsymbol{v}) := \nu \int_{\Omega_{\mathrm{o}}} \nabla \boldsymbol{u} : \nabla \boldsymbol{v} \, d\Omega, \quad \mathcal{B}(q, \boldsymbol{v}) := -\int_{\Omega_{\mathrm{o}}} q \nabla \cdot \boldsymbol{v} \, d\Omega \qquad (2.3)$$

and the linear form

$$\mathcal{F}(\boldsymbol{v}) := \int_{\Omega_{\mathrm{o}}} \boldsymbol{f} \cdot \boldsymbol{v} \, d\Omega. \qquad (2.4)$$

Then (2.2) can be compactly written as

$$\begin{cases} \mathcal{A}(\boldsymbol{u}, \boldsymbol{v}) + \mathcal{B}(p, \boldsymbol{v}) = \mathcal{F}(\boldsymbol{v}) - \mathcal{A}(\widehat{\boldsymbol{g}}, \boldsymbol{v}) & \text{for all } \boldsymbol{v} \in \mathcal{V} \\ \mathcal{B}(q, \boldsymbol{u}) = -\mathcal{B}(q, \widehat{\boldsymbol{g}}) & \text{for all } q \in \mathcal{Q} \end{cases}. \qquad (2.5)$$

With our assumptions on the displacement function η the domain Ω_{o} is of class $C^{0,1}$ and the Stokes equations have a unique solution $(\boldsymbol{u}, p) \in \mathcal{V} \times \mathcal{Q}$ [15].

2.2 Structural model: the 1-d generalized string equation

Next we give the equations for the structural displacement function η. These equations are in the Lagrangian form on the undeformed configuration of the wall, which we identify as the interval $(0, L)$ in our simplified 1-d case. We assume the displacements are small and always in the normal direction of Γ_w, the tangential displacement being equal to zero. The equilibrium equation for the structural displacement is chosen as the second order equation with a fourth order perturbation (with $\varepsilon > 0$ small)

$$\varepsilon \frac{\partial^4 \eta}{\partial x_1^4} - kGh \frac{\partial^2 \eta}{\partial x_1^2} + \frac{Eh}{1 - \nu_P^2} \frac{\eta}{R_0(x_1)^2} = \tau_{\Gamma_w}, \quad x_1 \in (0, L) \qquad (2.6)$$

where h is the wall thickness, k is the Timoshenko shear correction factor, G the shear modulus, E the Young modulus, ν_P the Poisson ratio, R_0 the radius of the reference configuration, and τ_{Γ_w} denotes the applied traction. This is a simplified 1-d equation for the structure that is often used in haemo-dynamic fluid-structure interaction problems as a "first approximation" [42].

We have added a fourth order term in order to have added regularity for the displacement. The weak form of (2.6) is to find the structural displacement in the normal direction $\eta \in \mathcal{D}$ s.t.

$$\tau_{\Gamma_w}(\phi) = \varepsilon \int_0^L \frac{\partial^2 \eta}{\partial x_1^2} \frac{\partial^2 \phi}{\partial x_1^2} dx_1 + kGh \int_0^L \frac{\partial \eta}{\partial x_1} \frac{\partial \phi}{\partial x_1} dx_1 + \frac{Eh}{1-\nu_P^2} \int_0^L \frac{\eta \phi}{R_0(x_1)^2} dx_1 := C(\eta, \phi) \tag{2.7}$$

for all ϕ in the space $\mathcal{D} := H_0^2(0, L)$ of kinematically admissible displacements.

2.3 Coupling of fluid and structure

The fluid and structure are coupled together by taking the applied traction τ_{Γ_w} to be the normal component of the normal Cauchy stress of the fluid on Γ_w, i.e.

$$\tau_{\Gamma_w} = (\boldsymbol{\sigma n}) \cdot \boldsymbol{n}, \quad \text{on } \Gamma_w. \tag{2.8}$$

This can be expressed in the weak sense using the residual $\mathcal{R}(\,\cdot\,; \boldsymbol{u}, p) \in X'_w$ of the fluid solution on the interface defined as [27]

$$\mathcal{R}(\boldsymbol{v}; \boldsymbol{u}, p) := F(\boldsymbol{v}) - \mathcal{A}(\boldsymbol{u} + \widehat{\boldsymbol{g}}, \boldsymbol{v}) - \mathcal{B}(p, \boldsymbol{v}) \quad \text{for } \boldsymbol{v} \in X_w \tag{2.9}$$

in the space of test functions $X_w := \{\boldsymbol{v} \in [H^1(\Omega_o)]^2 : \boldsymbol{v} \equiv 0 \text{ on } \Gamma_{in}\}$, or more precisely its Riesz representant $\boldsymbol{r}(\boldsymbol{u}, p) \in X_w$, and the trace operator $\gamma_{\Gamma_w} : X_w \to [H^{1/2}(\Gamma_w)]^2$ that transfers velocity test functions to structural test functions by taking the trace on Γ_w. Finally the entire steady fluid-structure interaction model can be written as follows: find $(\boldsymbol{u}, p, \eta) \in \mathcal{V} \times \mathcal{Q} \times \mathcal{D}$ s.t.

$$\begin{cases} \mathcal{A}(\boldsymbol{u}, v) + \mathcal{B}(p, \boldsymbol{v}) & = \mathcal{F}(\boldsymbol{v}) - \mathcal{A}(\widehat{\boldsymbol{g}}, v) & \forall \boldsymbol{v} \in \mathcal{V}(\eta) \\ \mathcal{B}(q, \boldsymbol{u}) & = -\mathcal{B}(q, \widehat{\boldsymbol{g}}) & \forall q \in \mathcal{Q}(\eta) \\ \mathcal{C}(\eta, \phi) & = \langle \gamma_{\Gamma_w}(\boldsymbol{r}(\boldsymbol{u}, p)) \cdot \boldsymbol{n}, \phi \rangle_{H^{-1/2}(0,L) \times H^{1/2}(0,L)} & \forall \phi \in \mathcal{D} \end{cases} . \tag{2.10}$$

Theorem 1 *With the assumptions outlined above, the coupled fluid-structure interaction problem (2.10) has at least one solution $(\boldsymbol{u}^*, p^*, \eta^*) \in \mathcal{V} \times \mathcal{Q} \times \mathcal{D}$.*

The proof is with the Schauder fixed point theorem; we refer to [17, 18] for the details. By standard arguments it also follows that if the problem data are Lipschitz continuous with sufficiently small Lipschitz constant, then the fixed point map is a strict contraction and the fixed point is unique.

Remark 2.1 *The displacement in (2.10) satisfies $\eta \in C^{1,1}\overline{(0, L)}$ so that $\Omega_o(\eta)$ is piecewise $C^{1,1}$ with convex corners. If in addition we have $\boldsymbol{g} \in H^{3/2}(\Gamma)$ then this is sufficient to obtain added regularity for the Stokes solution [16]. In this case the Stokes solution satisfies $(\boldsymbol{u}, p) \in [H^2(\Omega_o)]^2 \cap \mathcal{V} \times H^1(\Omega_o) \cap \mathcal{Q}$. However, this doesn't permit dropping the fourth order term*

in (2.6) since $C^{0,1}$ continuity of the displacement (and consequently the domain) would be lost. In cardiovascular applications the fourth order term is unphysically stiff for accurate modelling of vessel wall dynamics, and should be compensated for by choosing ε very small. In [25] we experimented with a second order equation for the structure. In addition to the aforementioned lack of regularity, the second order model lacks the ability to set boundary conditions on both the displacement and its derivative at the endpoints.

3 Parametric fluid equations in a fixed domain

To remove the difficulty of dealing with variable domains $\Omega_o(\eta)$ depending on the displacement η we rewrite the fluid equations in a fixed domain.

3.1 Parametric transformation to a fixed reference domain

Let Ω be a fixed reference domain at least of class $C^{0,1}$ and consider parametric maps $T(\boldsymbol{\mu}, \widetilde{\boldsymbol{x}}) \in C^\infty(\mathcal{D}; C^1(\Omega))$ that for each finite-dimensional vector of parameters $\boldsymbol{\mu}$ that belong to some admissible bounded and closed parameter range $\mathcal{P} \subset \mathbb{R}^P$ gives a smooth and invertible map $T(\boldsymbol{\mu}, \cdot) : \Omega \to \Omega_o(\boldsymbol{\mu})$. As a result the range of possible configurations of the fluid domain depends solely on the parameter, and all our admissible domain shapes are diffeomorphic images of the reference domain, see. Tildes are used above coordinates defined on the reference domain Ω to distinguish them from the corresponding coordinates defined on the original domain $\Omega_o(\boldsymbol{\mu})$, i.e. $T(\boldsymbol{\mu}, \widetilde{\boldsymbol{x}}) = \boldsymbol{x}$. Denoting by $J_T := \nabla_{\widetilde{\boldsymbol{x}}} T$ the Jacobian matrix of $T = (T_1, T_2)$ w.r.t the spatial variables we define the parametric transformation tensors for the viscous term

$$\nu_T(\boldsymbol{\mu}, \widetilde{\boldsymbol{x}}) \; := \; J_T^{-t}(\boldsymbol{\mu}, \widetilde{\boldsymbol{x}}) J_T^{-1}(\boldsymbol{\mu}, \widetilde{\boldsymbol{x}}) \det(J_T(\boldsymbol{\mu}, \widetilde{\boldsymbol{x}})) \tag{3.11}$$

and the pressure-divergence term (also known as the Piola transformation)

$$\chi_T(\boldsymbol{\mu}, \widetilde{\boldsymbol{x}}) \; := \; J_T^{-1}(\boldsymbol{\mu}, \widetilde{\boldsymbol{x}}) \det(J_T(\boldsymbol{\mu}, \widetilde{\boldsymbol{x}})) \tag{3.12}$$

respectively. We introduce the parametric bilinear forms on the fixed domain

$$\widetilde{\mathcal{A}}(\widetilde{\boldsymbol{u}}, \widetilde{\boldsymbol{v}}; \boldsymbol{\mu}) := \nu \int_\Omega (\nu_T(\boldsymbol{\mu}) \nabla \widetilde{\boldsymbol{u}}) : \nabla \widetilde{\boldsymbol{v}} d\Omega, \quad \widetilde{\mathcal{B}}(\widetilde{q}, \widetilde{\boldsymbol{v}}; \boldsymbol{\mu}) := - \int_\Omega \widetilde{q} \nabla \cdot (\chi_T(\boldsymbol{\mu}) \widetilde{\boldsymbol{v}}) d\Omega. \tag{3.13}$$

and the linear form

$$\widetilde{\mathcal{F}}(\widetilde{\boldsymbol{v}}; \boldsymbol{\mu}) := \int_\Omega \boldsymbol{f}(T(\boldsymbol{\mu}, \widetilde{\boldsymbol{x}})) \cdot \widetilde{\boldsymbol{v}} \det(J_T(\boldsymbol{\mu}, \widetilde{\boldsymbol{x}})) \, d\Omega. \tag{3.14}$$

The spaces $\widetilde{\mathcal{V}} := [H^1_{\Gamma_d}(\Omega)]^2$ and $\widetilde{\mathcal{Q}} := L^2(\Omega)$ do not depend on the parameter. Now the Stokes system (2.5) can be transformed back to the reference

7

domain, and we obtain the parametric Stokes equations on a fixed domain to find $(\widetilde{\boldsymbol{u}}(\boldsymbol{\mu}), \widetilde{p}(\boldsymbol{\mu})) \in \widetilde{\mathcal{V}} \times \widetilde{\mathcal{Q}}$

$$\begin{cases} \widetilde{\mathcal{A}}(\widetilde{\boldsymbol{u}}, \widetilde{\boldsymbol{v}}; \boldsymbol{\mu}) + \widetilde{\mathcal{B}}(\widetilde{p}, \widetilde{\boldsymbol{v}}; \boldsymbol{\mu}) = \widetilde{\mathcal{F}}(\widetilde{\boldsymbol{v}}; \boldsymbol{\mu}) - \widetilde{\mathcal{A}}(\widetilde{\boldsymbol{g}}, \widetilde{\boldsymbol{v}}; \boldsymbol{\mu}) & \text{for all } \widetilde{\boldsymbol{v}} \in \widetilde{\mathcal{V}} \\ \widetilde{\mathcal{B}}(\widetilde{q}, \widetilde{\boldsymbol{u}}; \boldsymbol{\mu}) = -\widetilde{\mathcal{B}}(\widetilde{q}, \widetilde{\boldsymbol{g}}; \boldsymbol{\mu}) & \text{for all } \widetilde{q} \in \widetilde{\mathcal{Q}} \end{cases} . \quad (3.15)$$

To obtain a parametric fluid domain that is compatible with the structural model, we assume Ω is chosen as the unperturbed configuration of the axisymmetric channel, $\Omega = (0, L) \times (0, R_0)$. While the structural equations are in the Lagrangian formulation, and therefore already written in the reference configuration, we make use of the parametric displacement function $\eta(\boldsymbol{\mu})$ that in our simplified case can be written as

$$\eta(x_1; \boldsymbol{\mu}) = T_2(\boldsymbol{\mu}; \begin{bmatrix} x_1 & R_0 \end{bmatrix}^t) - R_0, \quad \text{for } x_1 \in [0, L]. \quad (3.16)$$

3.2 Free-form deformations for flexible shape parameterizations

To define the free-form deformations we assume again that there exists a reference geometry Ω and look for a parametric family of smooth deformations $T_{\text{FFD}}(\boldsymbol{\mu})$ that can act on any kind of shape. Let $\Omega \subset D$ be embedded inside a control parallelogram D, which can be mapped affinely onto the unit square, $\Psi(D) = (0, 1) \times (0, 1)$ with coordinates $0 \le \xi_1, \xi_2 \le 1$. We overlay on the unit square a regular $(K + 1) \times (L + 1)$ grid of control points, where the location of each control point depends only on two scalar components of $\boldsymbol{\mu}$ according to

$$\boldsymbol{P}_{k,\ell}(\mu_{p(k,\ell)}, \mu_{p(k,\ell)+1}) := \begin{bmatrix} k/K + \mu_{p(k,\ell)} \\ \ell/L + \mu_{p(k,\ell)+1} \end{bmatrix} \quad (3.17)$$

where $p(k, \ell) := 2(K + 1)\ell + 2k + 1$ is a condensed index into the parameter vector $\boldsymbol{\mu}$ with a total of $2(K + 1)(L + 1)$ scalar components. Then we can define

$$\widehat{T}_{\text{FFD}}(\boldsymbol{\mu}; \boldsymbol{\xi}) := \sum_{k=0}^{K} \sum_{\ell=1}^{L} b_{k,\ell}^{K,L}(\xi_1, \xi_2) \boldsymbol{P}_{k,\ell}(\mu_{p(k,\ell)}, \mu_{p(k,\ell)+1}) \quad (3.18)$$

a smooth, invertible "deformation of identity" map $\widehat{T}_{\text{FFD}}$ for each $\boldsymbol{\mu}$ in a neighborhood of $\boldsymbol{0}$. The functions $b_{k,\ell}$ are tensor products of the Bernstein basis polynomials defined as

$$b_{k,\ell}^{K,L}(\xi_1, \xi_2) := \binom{K}{k} \binom{L}{\ell} \xi_1^k (1 - \xi_1)^{K-k} \xi_2^\ell (1 - \xi_2)^{L-\ell} \quad (3.19)$$

for $k = 0, \dots, K$ and $\ell = 0, \dots, L$, forming a total of $(K + 1)(L + 1)$ basis polynomials. By using the affine maps Ψ, Ψ^{-1} to map between the unit
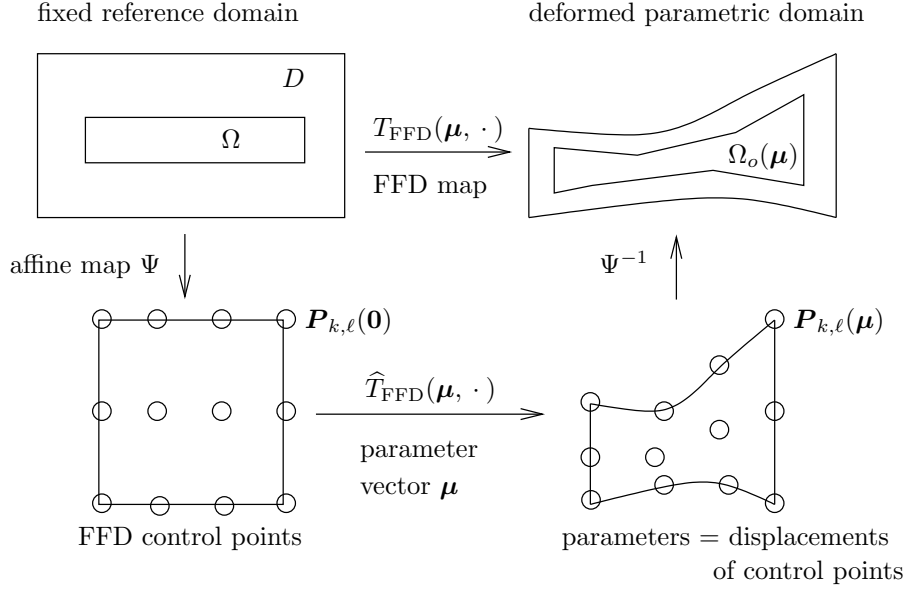
8

Figure 2: Schematic of the control points and resulting free-form parametric deformation

square and the original control parallelogram we can define the parametric free-form deformation map $T_{\mathrm{FFD}}(\boldsymbol{\mu}) := \Psi^{-1} \circ \widehat{T}(\boldsymbol{\mu}) \circ \Psi$. The parametric domains are then obtained from the restriction $\Omega_{\mathrm{o}}(\boldsymbol{\mu}) := T_{\mathrm{FFD}}(\boldsymbol{\mu}; \Omega)$.

In Fig. 2 we display a schematic diagram of the free-form deformations. Using the definition and the fact that the Bernstein basis polynomials form a partition of unity it can be shown that $T_{\mathrm{FFD}}(\mathbf{0}) = I$. Evaluation of the Bernstein basis polynomials (and subsequently T_{FFD} and its Jacobian matrix) can be performed in a numerically stable fashion using the recursive de Casteljau algorithm [9] without explicitly evaluating the formulas for T_{FFD}. In case there is a need to reduce the number of geometric parameters, we can keep fixed a number of control points or only allow them to move in one dimension. This allows the user to keep the number of FFD parameters to a desired low level (in our case roughly 5-10 parameters).

4 Parametric coupling of fluid and structure

We now introduce the computational algorithm for the solution of the coupled fluid-structure interaction problem.

4.1 Formulation of the coupled problem in the parameter space

Define the resolvant operator $\mathcal{L}_f : \mathcal{D} \to \mathcal{V} \times \mathcal{Q}$ giving for each displacement η and corresponding fluid domain $\Omega_o(\eta)$ the velocity-pressure solution pair by solving the equation (2.5), the trace operator $\mathcal{L}_r : \mathcal{V} \times \mathcal{Q} \to H^{-1/2}(0, L)$ taking the normal component of the Cauchy stress on the interface Γ_w computed from the fluid residual according to (2.9), and the resolvant operator $\mathcal{L}_s : H^{-1/2}(0, L) \to \mathcal{D}$ that provides the structural displacement for a given applied traction. The nonlinear equation system (2.10) is equivalent to the following fixed-point problem: find $\eta \in \mathcal{D}$ s.t.

$$(I - \mathcal{L}_s \circ \mathcal{L}_r \circ \mathcal{L}_f)(\eta) = 0. \tag{4.20}$$

We can alternatively formulate the fluid-structure problem (4.20) as a minimization problem:

$$\min_{\eta \in \mathcal{D}} \quad \| (I - \mathcal{L}_s \circ \mathcal{L}_r \circ \mathcal{L}_f)(\eta) \|_{\mathcal{D}}^2. \tag{4.21}$$

Any solution of (4.20) is also a minimizer of (4.21). A simplified parametrized version of (3.15) can be given as follows: find $\boldsymbol{\mu} \in \mathcal{P}$ that minimizes

$$\min_{\boldsymbol{\mu} \in \mathcal{P}} \quad \| (I - \mathcal{L}_s \circ \mathcal{L}_r \circ \mathcal{L}_f)(\eta(\boldsymbol{\mu})) \|_{\mathcal{D}}^2, \tag{4.22}$$

but this time we expect that the compatibility between the traction applied by fluid and the structural displacement is only achieved in a least-squares sense. The "quality of fit" depends on the dimension of the parameter space $\mathcal{P}$ as well as the approximation properties of the parametrization method. We call this the *parametric coupling* approach. The parametric coupling approach was used in [33] to solve the same problem, with the exception that there the applied traction (depending on this case only on the pressure profile on the wall) was directly parametrized.

Replacing the true displacement with its parametric counterpart can be understood as a nearest point projection step from the space of all kinematically admissible displacements $\mathcal{D}$ to the subset of parametrically admissible displacements, $\mathcal{D}_{\mathcal{P}} := \{\eta \in \mathcal{D} : \eta = \eta(\boldsymbol{\mu}), \boldsymbol{\mu} \in \mathcal{P}\}$, given by the operator $\mathcal{L}_p : \mathcal{D} \to \mathcal{D}_{\mathcal{P}}$ defined as $\mathcal{L}_p(\eta) := \arg \min_{\eta^* \in \mathcal{D}_{\mathcal{P}}} \|\eta - \eta^*\|_{\mathcal{D}}$. We then find the equivalent formulation of (4.22) being: find $\boldsymbol{\mu} \in \mathcal{P}$ s.t.

$$(I - \mathcal{L}_p \circ \mathcal{L}_s \circ \mathcal{L}_r \circ \mathcal{L}_f)(\eta(\boldsymbol{\mu})) = 0. \tag{4.23}$$

Remark 4.1 *To prove an equivalent to Theorem 1 for the parametrically coupled problem, we need to adapt the Schauder fixed-point argument. This*

requires showing that the nearest point projection is continuous in the strong H^2-norm topology. A sufficient condition for the continuity of the parametric projection is that the set of parametric displacements $\mathcal{D}_\mathcal{P} \subset \mathcal{D}$ be closed and convex. This is indeed the case in our FFD parametrized model problem when the parameter space $\mathcal{P}$ is closed and convex.

4.2 Finite element discretization of the Stokes equations

In order to give a computable algorithm for the solution of the parametrically coupled problem (4.23), we introduce discrete approximation spaces for the velocity $\widetilde{\mathcal{V}}_h \subset \widetilde{\mathcal{V}}$, pressure $\widetilde{\mathcal{Q}}_h \subset \widetilde{\mathcal{Q}}$, and structural displacement $\mathcal{D}_h \subset \mathcal{D}$ respectively. The first two spaces can be obtained by e.g. Taylor-Hood or mini finite element [43] discretization on a suitably regular mesh on the domain Ω; the latter is typically discretized with cubic Hermite elements that are C^1-continuous. Because a fixed mesh on Ω is used to solve the fluid equations for different parameter values, the combined dimension $\dim(\widetilde{\mathcal{V}}_h) + \dim(\widetilde{\mathcal{Q}}_h) = \mathcal{N}_v + \mathcal{N}_p =: \mathcal{N}_f$ of the finite element spaces should be chosen large enough that for the entire parameter range $\mathcal{P}$ the finite element solution of

$$\begin{cases} \widetilde{\mathcal{A}}(\widetilde{\boldsymbol{u}}_h, \widetilde{\boldsymbol{v}}_h; \boldsymbol{\mu}) + \widetilde{\mathcal{B}}(\widetilde{p}_h, \widetilde{\boldsymbol{v}}_h; \boldsymbol{\mu}) = \widetilde{\mathcal{F}}(\widetilde{\boldsymbol{v}}_h; \boldsymbol{\mu}) - \widetilde{\mathcal{A}}(\widetilde{\boldsymbol{g}}_h, \widetilde{\boldsymbol{v}}_h; \boldsymbol{\mu}) & \text{for all } \widetilde{\boldsymbol{v}}_h \in \widetilde{\mathcal{V}}_h \\ \widetilde{\mathcal{B}}(\widetilde{q}_h, \widetilde{\boldsymbol{u}}_h; \boldsymbol{\mu}) = -\widetilde{\mathcal{B}}(\widetilde{q}_h, \widetilde{\boldsymbol{g}}_h; \boldsymbol{\mu}) & \text{for all } \widetilde{q}_h \in \widetilde{\mathcal{Q}}_h \end{cases}$$

(4.24)

accurately represents the fluid solutions for the entire range of the parameter $\boldsymbol{\mu}$. While in the worst case this dictates that the finite element mesh needs to be refined uniformly everywhere, in Sect. 5 we will see that the reduced basis method alleviates the requirement of choosing a very large $\mathcal{N}_f$. By $\mathcal{N}_s$ we denote the dimension of the structural displacement approximation space. We have corresponding bases $\{\Psi_v^i\}_{i=1}^{\mathcal{N}_v}$, $\{\Psi_p^i\}_{i=1}^{\mathcal{N}_p}$, and $\{\Psi_\eta^i\}_{i=1}^{\mathcal{N}_s}$ for each finite element space. The matrices $\underline{A}(\boldsymbol{\mu}) \in \mathbb{R}^{\mathcal{N}_v \times \mathcal{N}_v}$, $\underline{B}(\boldsymbol{\mu}) \in \mathbb{R}^{\mathcal{N}_v \times \mathcal{N}_p}$, and $\underline{C} \in \mathbb{R}^{\mathcal{N}_s \times \mathcal{N}_s}$ corresponding to the discrete operators in the finite element basis are defined elementwise as

$$[\underline{A}(\boldsymbol{\mu})]_{i,j} = \widetilde{\mathcal{A}}(\Psi_v^j, \Psi_v^i; \boldsymbol{\mu}), \quad [\underline{B}(\boldsymbol{\mu})]_{i,j} = \widetilde{\mathcal{B}}(\Psi_p^j, \Psi_v^i; \boldsymbol{\mu}), \quad [\underline{C}]_{i,j} = \mathcal{C}(\Psi_\eta^j, \Psi_\eta^i)$$

(4.25)

and the right-hand side is given by $[\underline{F}(\boldsymbol{\mu})]_i = \langle \widetilde{F}, \Psi_v^i \rangle$. Similarly we denote the vectorial counterparts of the variables $[\underline{\widetilde{\boldsymbol{u}}}]_i = \widetilde{\boldsymbol{u}}_h(x_i)$, $[\underline{\widetilde{p}}]_i = \widetilde{p}_h(x_i)$, and $[\underline{\eta}]_i = \eta_h(x_i)$. We will also need the structural mass matrix $\underline{M} \in \mathbb{R}^{\mathcal{N}_s \times \mathcal{N}_s}$ defined as $[\underline{M}]_{i,j} = \int_0^L \Psi_\eta^j \Psi_\eta^i \, d\Gamma$.

4.3 Parametric coupling algorithm for the discrete problem

In order to transfer the load applied by the fluid to the structure in the discrete equations, we need to construct a discrete trace operator that returns the normal component of the trace of any velocity test function on the free

boundary. When the finite element spaces for the velocity and structural displacement are incompatible (because they feature either different order polynomials or they sit on nonconforming grids) one good strategy is to perform an L^2-projection between the two spaces. The discrete trace operator $G : \widetilde{\mathcal{V}}_h \to \mathcal{D}_h$ is thus defined according to

$$\int_0^L (G\widetilde{\boldsymbol{v}}_h)\, w_h\, d\Gamma = \int_0^L (\gamma_{\Gamma_w}(\widetilde{\boldsymbol{v}}_h) \cdot \boldsymbol{n})\, w_h\, d\Gamma \quad \text{for all } w_h \in \mathcal{D}_h. \quad (4.26)$$

In matrix form we have $\underline{G} := \underline{M}^{-1}\underline{\Gamma}$, where $[\underline{\Gamma}]_{i,j} = \int_0^L (\gamma_{\Gamma_w}(\Psi_v^j) \cdot \boldsymbol{n})\Psi_\eta^i$. This is a mortar-like approach in which $\mathcal{D}_h$ plays the role of slave space, see [44].

After the discrete trace operator has been formed, we can introduce a discrete version of the parametric coupled problem. Algorithm 4.1 computes a solution to the coupled problem by a fixed point iteration applied to the discretized equation (4.23). The nearest point projection is done

---

Algorithm 4.1 Parametric coupling of fluid and structure

Require: initial guess $\boldsymbol{\mu}^0$
1: Let $n = 0$.
2: **repeat**
3:     Solve the discretized Stokes equations for $\widetilde{\boldsymbol{u}}_h^n = \widetilde{\boldsymbol{u}}_h(\boldsymbol{\mu}^n)$ and $\widetilde{p}_h^n = \widetilde{p}_h(\boldsymbol{\mu}^n)$
4:     Form the discrete fluid residual

$$\underline{R}_h(\widetilde{\boldsymbol{u}}_h, \widetilde{p}_h; \boldsymbol{\mu}) = \underline{F}(\boldsymbol{\mu}^n) - \underline{A}(\boldsymbol{\mu}^n)\left[\widetilde{\underline{u}}_h^n + \widetilde{\underline{g}}_h\right] - \underline{B}(\boldsymbol{\mu}^n)\widetilde{\underline{p}}_h^n.$$

5:     Form the discrete trace operator $\underline{G}$.
6:     Solve the structural equations for the assumed displacement $\widehat{\underline{\eta}}_h$ from $\underline{C}\widehat{\underline{\eta}}_h = \underline{G}\underline{R}_h(\widetilde{\boldsymbol{u}}_h, \widetilde{p}_h; \boldsymbol{\mu}^n)$.
7:     Solve the constrained minimization problem in the parameter space

$$\min_{\boldsymbol{\mu}^{n+1} \in \mathcal{P}} \quad \left[\widehat{\underline{\eta}}_h - \underline{\eta}_h(\boldsymbol{\mu}^{n+1})\right]^t \underline{C} \left[\widehat{\underline{\eta}}_h - \underline{\eta}_h(\boldsymbol{\mu}^{n+1})\right]$$

       to obtain the next configuration parameter $\boldsymbol{\mu}^{n+1}$.
8:     Set $n \to n + 1$.
9: **until** stopping criteria $|\boldsymbol{\mu}^{n+1} - \boldsymbol{\mu}^n| < \text{TOL}$ is met.

---

by minimizing a least-squares functional, and involves no further fluid or structure solutions during the optimization loop. Since the analytic form (3.16) of the parametric displacement function $\underline{\eta}_h(\boldsymbol{\mu})$ is available, the first- and second-order sensitivities are readily available, and the parametric projection step can be efficiently performed using affine-scaling interior-point Newton methods [7] for nonlinear programming with box constraints.

4.4 A priori convergence as the number of parameters increases

The coupling accuracy that is obtainable with the parametric coupling formulation depends mostly on the approximation properties of the parametric map $T(\boldsymbol{\mu}, \cdot)$. If the parametric displacements $\eta(\boldsymbol{\mu})$ form a linear subspace $\mathcal{D}_{\mathcal{P}} \subset \mathcal{D}$, the concept of (Kolmogorov) N-width [38] can be used to measure the asymptotic approximation obtainable as the number of parameters $P \to \infty$. Let X be a Banach-space endowed with norm $|| \cdot ||_X$, $Y \subset X$ its bounded subset whose elements we are trying to approximate, and denote by $X_n \subset X$ any linear subspace of dimension n. The optimal N-width of the set Y in the space X is defined as

$$d_n(Y; X) = \inf_{X_n, \dim(X_n) = n} \sup_{y \in Y} \inf_{x \in X_n} ||x - y||_X \qquad (4.27)$$

and the space X_n^* that gives the infimum is the optimal subspace of dimension n for approximating Y. In the case that $X = L^2(0, L)$ and

$$Y = \{y \in H_0^2(0, L) \ : \ ||y||_2 \leq 1\} \qquad (4.28)$$

it is known that the optimal subspace has N-width $d_n(X, Y) = \lambda_n^{-1/2}$, where $0 < \lambda_1 < \lambda_2 < \ldots$ are the positive eigenvalues of an Euler-Bernoulli boundary-value problem: find $(y_k, \lambda_k) \in H_0^2(0, L) \times \mathbb{R}^+$ s.t.

$$(y_k^{(2)}, w^{(2)})_{L^2} = \lambda_k (y_k, w)_{L^2} \quad \text{for } k = 1, 2, \ldots . \qquad (4.29)$$

An optimal subspace X_n^* is spanned by the first n eigenfunctions y_k. The N-width theory is useful in that it gives the an estimate of the worst case asymptotic convergence rate of an approximation to the structural displacement as the number of parameters $P \to \infty$. The eigenvalues $\lambda_k = \ell_k^4$ of (4.29) are solutions of (see e.g. [4])

$$1 - (\cos \ell_k L)(\cosh \ell_k L) = 0, \qquad (4.30)$$

they grow like $\ell_k \approx (2k + 1)\frac{\pi}{2L}$, so that in this case the N-width in the L^2-norm behaves like $O(P^{-2})$.

5 Reduced basis for steady incompressible Stokes

The most computationally expensive part of Algorithm 4.1 is step 3, that is, the solution of the parametric Stokes equations. With the assumption of small, C^∞ geometric deformations the dependence of the solutions of the Stokes equations on the parameter is also "smooth" in the sense that the manifold of parametric solutions in the space X is C^∞, and there are no bifurcation points leading to large qualitative changes in the velocity field.

With this assumption the reduced basis method can be reliably applied to reduce the problem to a much lower-dimensional subspace. It holds also for the Navier-Stokes equations when the parameter is e.g. the Reynolds number that is taken small enough. See [24, 37] for early development of the reduced basis method for Navier-Stokes equations, [6, 8, 54] for more recent results in a posteriori error estimation, and [41] for implementation details.

The reduced basis method consists of computing finite element solutions to the parametric PDEs at suitable parameter points and using their span to construct a low-dimensional approximation space for Galerkin projection. Let $\boldsymbol{\mu}^1, \boldsymbol{\mu}^2, \ldots, \boldsymbol{\mu}^N$ be a small collection of parametric configurations that form a good ensemble for approximating the behavior of the parametric fluid system in question. By computing the finite element snapshot solutions $(\widetilde{\boldsymbol{u}}_h(\boldsymbol{\mu}^n), \widetilde{p}_h(\boldsymbol{\mu}^n))$ s.t.

$$
\begin{cases}
\widetilde{\mathcal{A}}(\widetilde{\boldsymbol{u}}_h, \widetilde{\boldsymbol{v}}_h; \boldsymbol{\mu}^n) + \widetilde{\mathcal{B}}(\widetilde{p}_h, \widetilde{\boldsymbol{v}}_h; \boldsymbol{\mu}^n) = \widetilde{\mathcal{F}}(\widetilde{\boldsymbol{v}}_h; \boldsymbol{\mu}^n) - \widetilde{\mathcal{A}}(\widetilde{\boldsymbol{g}}_h, \widetilde{\boldsymbol{v}}_h; \boldsymbol{\mu}^n) & \text{for all } \widetilde{\boldsymbol{v}}_h \in \widetilde{\mathcal{V}}_h \\
\widetilde{\mathcal{B}}(\widetilde{q}_h, \widetilde{\boldsymbol{u}}_h; \boldsymbol{\mu}^n) = -\widetilde{\mathcal{B}}(\widetilde{q}_h, \widetilde{\boldsymbol{g}}_h; \boldsymbol{\mu}^n) & \text{for all } \widetilde{q}_h \in \widetilde{\mathcal{Q}}_h
\end{cases}
\tag{5.31}
$$

for $n = 1, \ldots, N$ we can define the problem-dependent approximation spaces for velocity and pressure

$$
\begin{aligned}
\mathcal{V}_h^N &:= \operatorname{span}(\widetilde{\boldsymbol{u}}_h(\boldsymbol{\mu}^n) \ : \ n = 1, \ldots, N) \\
\mathcal{Q}_n^N &:= \operatorname{span}(\widetilde{p}_h(\boldsymbol{\mu}^n) \ : \ n = 1, \ldots, N)
\end{aligned},
\tag{5.32}
$$

which possess some spectral approximation properties [5]. Namely, if we construct a suitably orthonormalized bases $\{\boldsymbol{\zeta}_v^n\}_{n=1}^N$ and $\{\zeta_p^n\}_{n=1}^N$ for the spaces $\mathcal{V}_h^N$ and $\mathcal{Q}_n^N$ respectively and seek for a given $\boldsymbol{\mu} \in \mathcal{P}$ the Galerkin projection $(\widetilde{\boldsymbol{u}}_h^N(\boldsymbol{\mu}^n), \widetilde{p}_h^N(\boldsymbol{\mu}^n))$ s.t.

$$
\begin{cases}
\widetilde{\mathcal{A}}(\widetilde{\boldsymbol{u}}_h^N, \widetilde{\boldsymbol{v}}_h^N; \boldsymbol{\mu}) + \widetilde{\mathcal{B}}(\widetilde{p}_h^N, \widetilde{\boldsymbol{v}}_h^N; \boldsymbol{\mu}) = \widetilde{\mathcal{F}}(\widetilde{\boldsymbol{v}}_h^N; \boldsymbol{\mu}) - \widetilde{\mathcal{A}}(\widetilde{\boldsymbol{g}}_h, \widetilde{\boldsymbol{v}}_h^N; \boldsymbol{\mu}) & \text{for all } \widetilde{\boldsymbol{v}}_h^N \in \widetilde{\mathcal{V}}_h^N \\
\widetilde{\mathcal{B}}(\widetilde{q}_h^N, \widetilde{\boldsymbol{u}}_h^N; \boldsymbol{\mu}) = -\widetilde{\mathcal{B}}(\widetilde{q}_h^N, \widetilde{\boldsymbol{g}}_h; \boldsymbol{\mu}) & \text{for all } \widetilde{q}_h^N \in \widetilde{\mathcal{Q}}_h^N
\end{cases}
\tag{5.33}
$$

then the convergence of this reduced basis approximation, $(\widetilde{\boldsymbol{u}}_h^N, \widetilde{p}_h^N) \to (\widetilde{\boldsymbol{u}}_h, \widetilde{p}_h)$ as $N \to \infty$, is in the best case exponential in N [30] and in many applications very rapid for the entire parameter range $\boldsymbol{\mu} \in \mathcal{P}$. This means that the reduced basis dimension N can be chosen much smaller than the finite element space dimension, $N \ll \mathcal{N}_f$, and we expect that the reduced system of size $N \times N$ can be efficiently assembled and solved for any $\boldsymbol{\mu}$, and that its solution takes only negligible time and memory when compared to the cost of solving the finite element system of size $\mathcal{N}_f \times \mathcal{N}_f$. Three main aspects need to be addressed when using the reduced basis solution to approximate the underlying finite element solution:

1. Efficient methods for the assembly and solution of the reduced system (5.33).

2. Stability of the reduced basis Stokes approximation [50].

3. Certified a posteriori error bounds for the reduced basis solution [47].

The a posteriori estimate also gives us a way to choose the parameter values $\{\boldsymbol{\mu}^n\}_{n=1}^N$ that define the RB space by a greedy algorithm that explores the parameter space [20, 47].

5.1 Efficient solution of the RB system for affine problems

The computational setup typical for reduced basis methods is of *offline* vs. *online* stages. We are willing to spend extra computational effort that depends on the (a priori large) dimension of the finite element approximation space $\mathcal{N}_f$ and possibly takes considerable time (the offline stage), provided that once the necessary data structures have been precomputed and stored, we can then assemble and solve the reduced basis system inexpensively and with complexity only depending on N, but not on $\mathcal{N}_f$ (the online stage) for any parametric configuration. The same requirements hold for any a posteriori error estimates we obtain in the online stage.

In reduced basis methods an important assumption that facilitates splitting the problem into offline and online stages is usually made. We say that the parametric PDE problem is *affinely parametrized* if the bilinear forms satisfy

$$\widetilde{\mathcal{A}}(\widetilde{\boldsymbol{u}}, \widetilde{\boldsymbol{v}}; \boldsymbol{\mu}) = \sum_{q=1}^{Q_a} \Theta_q^a(\boldsymbol{\mu}) \widetilde{\mathcal{A}}_q(\widetilde{\boldsymbol{u}}, \widetilde{\boldsymbol{v}}), \quad \widetilde{\mathcal{B}}(\widetilde{p}, \widetilde{\boldsymbol{v}}; \boldsymbol{\mu}) = \sum_{q=1}^{Q_b} \Theta_q^b(\boldsymbol{\mu}) \widetilde{\mathcal{B}}_q(\widetilde{p}, \widetilde{\boldsymbol{v}}) \quad (5.34)$$

for some computable scalar functions Θ_q^a, Θ_q^b depending only on the parameters, and continuous bilinear forms $\widetilde{\mathcal{A}}_q$, $\widetilde{\mathcal{B}}_q$ depending only on the spatial variables, and if the linear form satisfies.

$$\widetilde{\mathcal{F}}(\widetilde{\boldsymbol{v}}; \boldsymbol{\mu}) = \sum_{q=1}^{Q_f} \Theta_q^f(\boldsymbol{\mu}) \widetilde{\mathcal{F}}_q(\widetilde{\boldsymbol{v}}) \quad (5.35)$$

for some computable scalar function Θ_q^f depending only on the parameters, and continuous linear forms $\widetilde{\mathcal{F}}_q$ depending only on the spatial variables. Accordingly we define the affinely decomposed matrices and right-hand sides

$$[\underline{A}_q]_{i,j} := \widetilde{\mathcal{A}}_q(\Psi_v^j, \Psi_v^i), \quad [\underline{B}_q]_{i,j} := \widetilde{\mathcal{B}}_q(\Psi_p^j, \Psi_v^i), \quad [\underline{\boldsymbol{f}}_q]_j := \widetilde{\mathcal{F}}_q(\Psi_v^j). \quad (5.36)$$

With assumption (5.34) the reduced basis problem splits into parameter-independent matrices and parameter-dependent scalar coefficient functions, and we obtain the linear system of $2N \times 2N$ equations to find $\widetilde{\underline{\boldsymbol{u}}}_h^N \in \mathbb{R}^N$ and

$\widetilde{p}_h^N \in \mathbb{R}^N$ s.t.

$$
\begin{bmatrix} \sum_{q=1}^{Q_a} \Theta_q^a(\boldsymbol{\mu})\underline{A}_q^N & \sum_{q=1}^{Q_b} \Theta_q^b(\boldsymbol{\mu})\underline{B}_q^N \\[2ex] \sum_{q=1}^{Q_b} \Theta_q^b(\boldsymbol{\mu})[\underline{B}_q^N]^t & \end{bmatrix} \begin{bmatrix} \widetilde{\underline{u}}_h^N \\[2ex] \widetilde{p}_h^N \end{bmatrix} = \begin{bmatrix} \underline{f}^N(\boldsymbol{\mu}) \\[2ex] \underline{g}^N(\boldsymbol{\mu}) \end{bmatrix}, \qquad (5.37)
$$

where the right-hand side is

$$
\begin{bmatrix} \underline{f}^N(\boldsymbol{\mu}) \\[2ex] \underline{g}^N(\boldsymbol{\mu}) \end{bmatrix} := \begin{bmatrix} \sum_{q=1}^{Q_f} \Theta_q^f(\boldsymbol{\mu})\underline{Z}_v\underline{f}_q - \sum_{q=1}^{Q_a} \Theta_q^a(\boldsymbol{\mu})\underline{A}_q^N \underline{Z}_v\widetilde{\underline{g}}_h \\[2ex] -\sum_{q=1}^{Q_b} \Theta_q^b(\boldsymbol{\mu})[\underline{B}_q^N]^t \underline{Z}_v\widetilde{\underline{g}}_h \end{bmatrix} \qquad (5.38)
$$

and the reduced basis matrices and vectors are defined as

$$
\begin{aligned}
[\underline{Z}_v]_{i,j} &:= \zeta_v^i(\boldsymbol{x}_j) & i &= 1,\ldots,N, \quad j = 1,\ldots,\mathcal{N}_v \\
[\underline{Z}_p]_{i,j} &:= \zeta_p^i(\boldsymbol{x}_j) & i &= 1,\ldots,N, \quad j = 1,\ldots,\mathcal{N}_p \\
[\underline{A}_q^N]_{i,j} &:= \underline{Z}_v\underline{A}_q\underline{Z}_v^t, & i,j &= 1,\ldots,N \\
[\underline{B}_q^N]_{i,j} &:= \underline{Z}_p\underline{B}_q\underline{Z}_v^t, & i,j &= 1,\ldots,N
\end{aligned} \qquad (5.39)
$$

where the matrices $\underline{Z}_v$, $\underline{Z}_p$, $\underline{A}_q^N$, and $\underline{B}_q^N$ are assembled once and stored. The system (5.37) can then be assembled and solved for any $\boldsymbol{\mu} \in \mathcal{P}$ with complexity not depending on $\mathcal{N}_f$ by simply evaluating the coefficient functions and summing the contributions from each term. If the affinity assumption is not in effect, the cost of the online evaluations increases and the reduced basis method becomes less attractive.

5.2 Empirical interpolation method for nonaffine problems

From the expressions (3.13) and (3.14) for the parametric bilinear forms it is clear that the bilinear form $\widetilde{\mathcal{A}}$ does not satisfy the affine parametrization assumption. In fact, most geometric parametrizations are nonaffine. One way to treat nonaffinely parametrized PDEs is to use a process called the Empirical Interpolation Method (EIM) [3, 19, 29]. An approximation to the nonaffinely parametrized bilinear forms $\widetilde{\mathcal{A}}$, $\widetilde{\mathcal{B}}$, and the linear form $\widetilde{\mathcal{F}}$ are sought in the form

$$
\widetilde{\mathcal{A}}(u,v;\boldsymbol{\mu}) = \sum_{q=1}^{Q_a} \Theta_a^q(\boldsymbol{\mu})\widetilde{\mathcal{A}}_q(\widetilde{u},\widetilde{v}) + \varepsilon_{\text{EIM}}^a(\widetilde{\boldsymbol{x}},\boldsymbol{\mu}),
$$

$$
\widetilde{\mathcal{B}}(u,v;\boldsymbol{\mu}) = \sum_{q=1}^{Q_b} \Theta_a^q(\boldsymbol{\mu})\widetilde{\mathcal{B}}_q(\widetilde{u},\widetilde{v}) + \varepsilon_{\text{EIM}}^b(\widetilde{\boldsymbol{x}},\boldsymbol{\mu}), \qquad (5.40)
$$

$$
\widetilde{\mathcal{F}}(v;\boldsymbol{\mu}) = \sum_{q=1}^{Q_f} \Theta_f^q(\boldsymbol{\mu})\widetilde{\mathcal{F}}_q(\widetilde{v}) + \varepsilon_{\text{EIM}}^f(\widetilde{\boldsymbol{x}},\boldsymbol{\mu}),
$$

that is, by suitable affine components plus suitable error terms $\varepsilon_{\text{EIM}}^a$, $\varepsilon_{\text{EIM}}^b$, $\varepsilon_{\text{EIM}}^f$ that need to be controlled to an acceptable tolerance. The idea is as follows: for any scalar function $g(\boldsymbol{x}, \boldsymbol{\mu}) \in C^s(\mathcal{P}; L^\infty(\Omega))$, with $s \geq 0$, the goal is to find an approximate expansion of the form

$$g_Q(\boldsymbol{x}, \boldsymbol{\mu}) = \sum_{q=1}^{Q} \Theta_q(\boldsymbol{\mu}) \psi_q(\boldsymbol{x}) \tag{5.41}$$

for which $\|g(\cdot, \boldsymbol{\mu}) - g_Q(\cdot, \boldsymbol{\mu})\|_{L^\infty(\Omega)} < \text{TOL}$ in the entire range of parameters $\boldsymbol{\mu} \in \mathcal{P}$. In the empirical interpolation one seeks a set of interpolation points $\boldsymbol{x}^q \in \Omega$ and a set of shape functions $\psi_q(\boldsymbol{x})$ s.t. the expansion (5.41) is obtained through solving the Lagrange interpolation problem

$$\sum_{q=1}^{Q} [\underline{\Upsilon}]_{q',q} [\underline{\Theta}]_j(\boldsymbol{\mu}) = g(\boldsymbol{x}^{q'}, \boldsymbol{\mu}), \quad \forall\, q' = 1, \dots, Q \tag{5.42}$$

where the interpolation matrix $\Upsilon \in \mathbb{R}^{Q \times Q}$ is defined elementwise as $[\underline{\Upsilon}]_{q',q} := \psi_q(\boldsymbol{x}^{q'})$ for $q, q' = 1, \dots, Q$. This can be done with the greedy algorithm detailed in [3, 29] that proceeds to construct a hierarchical sequence of approximation spaces. Using the EIM for each component of $[\nu_T]_{i,j}$ and combining the resulting approximate affine expansions

$$\mathcal{A}_q^{i,j}(\widetilde{\boldsymbol{u}}, \widetilde{\boldsymbol{v}}) = \nu \int_\Omega \psi_q^{i,j}(\boldsymbol{x}) \frac{\partial \widetilde{u}_j}{\partial x_i} \frac{\partial \widetilde{v}_j}{\partial x_i}\, dx, \quad \text{for } q = 1, \dots, Q^{i,j} \tag{5.43}$$

we get

$$\mathcal{A}(\widetilde{\boldsymbol{u}}, \widetilde{\boldsymbol{v}}; \boldsymbol{\mu}) = \sum_{i=1}^{2} \sum_{j=1}^{2} \sum_{q=1}^{Q^{i,j}} \Theta_q^{i,j}(\boldsymbol{\mu}) \mathcal{A}_q^{i,j}(\widetilde{\boldsymbol{u}}, \widetilde{\boldsymbol{v}}) \tag{5.44}$$

an expansion with a total of $Q_a := Q^{1,1} + Q^{1,2} + Q^{2,1} + Q^{2,2}$ terms, and similarly for the other forms. In practice the EIM has been quite useful for solving nonaffinely parametrized PDEs with the reduced basis method [19, 34, 45].

Remark 5.1 *For the free-form deformation detailed in Sect. 3.2 in fact the forms $\widetilde{\mathcal{B}}$ and $\widetilde{\mathcal{F}}$ are affine due to the fact that the map T_{FFD} is polynomial. This reduces the number of terms $Q_a + Q_b + Q_f$ needed in the approximate affine expansion, as was first observed in [48]. For generic nonpolynomial shape parametrizations the situation remains more challenging.*

5.3 Inf-sup stability of the reduced basis Stokes approximation

We briefly recall the general existence and uniqueness theory for noncoercive linear PDEs. Let X be a Hilbert-space endowed with the inner product

$(\, \cdot \, , \, \cdot \,)_X$ and the corresponding norm $|| \, \cdot \, ||_X := \sqrt{(\, \cdot \, , \, \cdot \,)_X}$. The general noncoercive PDE in weak form is: find $U \in X$ s.t.

$$\Phi(U, V) = F(V) \quad \text{for all } V \in X \tag{5.45}$$

where $\Phi : X \times X \to \mathbb{R}$ is a continuous, symmetric bilinear form and $F : X \to \mathbb{R}$ a continuous linear form. The Babuška inf-sup stability condition [2] that guarantees the existence of a unique solution is

$$\exists \varphi > 0 \, : \, \inf_{U \in X} \sup_{V \in X} \frac{\Phi(U, V)}{||U||_X ||V||_X} \geq \varphi, \tag{5.46}$$

and that solution satisfies a Lax-Milgram -type stability estimate

$$||U||_X \leq ||F||_{X'} / \varphi. \tag{5.47}$$

In our Stokes case we have $U = (\boldsymbol{u}, p)$, $V = (\boldsymbol{v}, q)$, the product space $X := \mathcal{V} \times \mathcal{Q}$, the norm $||V||_X^2 := ||\boldsymbol{v}||_{\mathcal{V}}^2 + ||q||_{\mathcal{Q}}^2$, and the bilinear form $\Phi(U, V) := \mathcal{A}(\boldsymbol{u}, \boldsymbol{v}) + \mathcal{B}(p, \boldsymbol{v}) + \mathcal{B}(q, \boldsymbol{u})$. The inf-sup constant φ in this case is the least singular value of the linear operator associated with the Stokes equation [14].

The stability of the continuous Stokes equations is well-known to not imply stability of the discretized Stokes equations for many "reasonable" finite element discretizations. The situation is similar in the reduced basis context. Rather than working directly with condition (5.46) it is customary to apply the so-called Babuška-Brezzi -theory that allows one to consider only the bilinear form $\mathcal{B}$. In a conforming finite element approximation the ellipticity of the bilinear form $\mathcal{A}$ is inherited by the discretized problem, and thus a sufficient condition for stability is that the finite element velocity and pressure spaces $\mathcal{V}_h$ and $\mathcal{Q}_h$ should be chosen such that they satisfy the discrete Ladyzhenskaya-Babuška-Brezzi (LBB) condition [15]

$$\exists \beta_h > 0 \, : \, \inf_{q_h \in \mathcal{Q}_h} \sup_{\boldsymbol{v} \in \mathcal{V}_h} \frac{\mathcal{B}(q, \boldsymbol{v})}{||\boldsymbol{v}||_{\mathcal{V}} ||q||_{\mathcal{Q}}} \geq \beta_h. \tag{5.48}$$

Popular choices of element pairs that satisfy this condition include the mini element ($\mathbb{P}_1 + \text{bubble}/\mathbb{P}_1$), and the Taylor-Hood $\mathbb{P}_{k+1}/\mathbb{P}_k$ family for $k \geq 1$. In the case of parametric Stokes equations on the reference domain Ω we require further that

$$\inf_{\widetilde{q}_h \in \widetilde{\mathcal{Q}}_h} \sup_{\widetilde{\boldsymbol{v}}_h \in \widetilde{\mathcal{V}}_h} \frac{\mathcal{B}(\widetilde{q}_h, \widetilde{\boldsymbol{v}}_h; \boldsymbol{\mu})}{||\widetilde{\boldsymbol{v}}_h||_{\widetilde{\mathcal{V}}} ||\widetilde{q}_h||_{\widetilde{\mathcal{Q}}}} = \widetilde{\beta}_h(\boldsymbol{\mu}) > 0 \quad \text{for all } \boldsymbol{\mu} \in \mathcal{P}. \tag{5.49}$$

When the parametrization arises from geometric transformations and $\mathcal{B}$ is given by (3.13), we can use (in the case that the transform tensor is computed exactly and not approximated by numerical quadratures) the divergence

of a vector field is invariant under the Piola transform and $\widetilde{\mathcal{B}}(\widetilde{q}, \widetilde{\boldsymbol{v}}; \boldsymbol{\mu}) = \mathcal{B}(q, \boldsymbol{v})$, for all $\boldsymbol{\mu} \in \mathcal{P}$; consequently $\widetilde{\beta}_h(\boldsymbol{\mu}) = \beta_h$. For the reduced basis approximation we have a similar inf-sup condition

$$\inf_{\widetilde{q}_h^N \in \widetilde{\mathcal{Q}}_h^N} \sup_{\widetilde{\boldsymbol{v}}_h^N \in \widetilde{\mathcal{V}}_h^N} \frac{\mathcal{B}(\widetilde{q}_h^N, \widetilde{\boldsymbol{v}}_h^N; \boldsymbol{\mu})}{||\widetilde{\boldsymbol{v}}_h^N||_{\widetilde{\mathcal{V}}} ||\widetilde{q}_h^N||_{\widetilde{\mathcal{Q}}}} = \widetilde{\beta}_h^N(\boldsymbol{\mu}) > 0 \quad \text{for all } \boldsymbol{\mu} \in \mathcal{P}, \qquad (5.50)$$

but unfortunately it is not in general true that (5.49) implies (5.50). One way to guarantee stability of the reduced basis Stokes system is to enrich the velocity space with supremizers defined using the supremizer operator [50, 45] $T^{\boldsymbol{\mu}} : \mathcal{Q}_h \to \mathcal{V}_h$ s.t.

$$(T^{\boldsymbol{\mu}} \widetilde{q}_h, \widetilde{\boldsymbol{v}}_h)_{\widetilde{\mathcal{V}}} = \widetilde{\mathcal{B}}(\widetilde{q}_h, \widetilde{\boldsymbol{v}}_h; \boldsymbol{\mu}) \quad \text{for all } \widetilde{\boldsymbol{v}}_h \in \widetilde{\mathcal{V}}_h. \qquad (5.51)$$

Note that the name "supremizer" comes from the property

$$\sup_{\widetilde{\boldsymbol{v}}_h \in \widetilde{\mathcal{V}}} \frac{\widetilde{\mathcal{B}}(\widetilde{q}_h, \widetilde{\boldsymbol{v}}_h; \boldsymbol{\mu})}{||\widetilde{\boldsymbol{v}}_h||_{\widetilde{\mathcal{V}}_h}} = \frac{\widetilde{\mathcal{B}}(\widetilde{q}_h, T^{\boldsymbol{\mu}} \widetilde{q}_h; \boldsymbol{\mu})}{||T^{\boldsymbol{\mu}} \widetilde{q}_h||_{\widetilde{\mathcal{V}}}}. \qquad (5.52)$$

If for each pressure basis function $\widetilde{p}_h^n$ we compute the corresponding supremizer velocity field

$$\widetilde{\boldsymbol{s}}_h^n(\boldsymbol{\mu}) := T^{\boldsymbol{\mu}} \widetilde{p}_h^n \qquad (5.53)$$

and add these to the velocity approximation basis

$$\widetilde{\mathcal{V}}_h^{N,\text{supr}}(\boldsymbol{\mu}) := \widetilde{\mathcal{V}}_h^N \oplus \text{span}(\widetilde{\boldsymbol{s}}_h^n(\boldsymbol{\mu}) : n = 1, \dots, N) \qquad (5.54)$$

we can replace in (5.50) the space $\widetilde{\mathcal{V}}_h^N$ with $\widetilde{\mathcal{V}}_h^{N,\text{supr}}(\boldsymbol{\mu})$ and prove (see [50]) that now $\widetilde{\beta}_h^N(\boldsymbol{\mu}) \geq \widetilde{\beta}_h(\boldsymbol{\mu})$ so that the supremizer-enriched velocity space $\widetilde{\mathcal{V}}_h^{N,\text{supr}}$ of dimension $2N$ inherits the inf-sup stability from the finite element problem. A difficulty related to the supremizers is that now the reduced velocity space depends explicitly on the parameter. In [50] a way to deal with this is proposed so that the explicit parameter dependence is lost. The condition $\widetilde{\beta}_h(\boldsymbol{\mu}) > 0$ then implies that both $\widetilde{\varphi}_h(\boldsymbol{\mu}) > 0$ and $\widetilde{\varphi}_h^N(\boldsymbol{\mu}) > 0$. For further study of the relationship between the different stability constants and the a posteriori estimator given above, we refer to [46].

5.4 A posteriori error bounds for the reduced basis solution

Denoting the error between the finite element solution and its reduced basis approximation both for the velocity and pressure as $\boldsymbol{e}_u := \widetilde{\boldsymbol{u}}_h - \widetilde{\boldsymbol{u}}_h^N$ and $e_p := \widetilde{q}_h - \widetilde{q}_h^N$, we define the combined residual as

$$\mathcal{R}_{\boldsymbol{\mu}}(\widetilde{\boldsymbol{v}}_h, \widetilde{q}_h) := \widetilde{\mathcal{A}}(\boldsymbol{e}_u(\boldsymbol{\mu}), \widetilde{\boldsymbol{v}}_h; \boldsymbol{\mu}) + \widetilde{\mathcal{B}}(e_p(\boldsymbol{\mu}), \widetilde{\boldsymbol{v}}_h; \boldsymbol{\mu}) + \widetilde{\mathcal{B}}(\widetilde{q}_h, \boldsymbol{e}_u(\boldsymbol{\mu}); \boldsymbol{\mu}) \quad \forall (\widetilde{\boldsymbol{v}}_h, \widetilde{q}_h) \in X_h.$$
$$(5.55)$$

Then $\mathcal{R}_{\boldsymbol{\mu}}(\widetilde{\boldsymbol{v}}_h, \widetilde{q}_h) \in X_h'$ and satisfies

$$\mathcal{R}_{\boldsymbol{\mu}}(\widetilde{\boldsymbol{v}}_h, q_h) = \mathcal{F}(\widetilde{\boldsymbol{v}}_h; \boldsymbol{\mu}) - \widetilde{\mathcal{A}}(\widetilde{\boldsymbol{u}}_h^N, \widetilde{\boldsymbol{v}}; \boldsymbol{\mu}) + \widetilde{\mathcal{B}}(\widetilde{q}_h^N, \widetilde{\boldsymbol{v}}_h; \boldsymbol{\mu}) + \widetilde{\mathcal{B}}(\widetilde{q}_h, \widetilde{\boldsymbol{u}}_h^N; \boldsymbol{\mu}) \quad \forall(\widetilde{\boldsymbol{v}}_h, \widetilde{q}_h) \in X_h \tag{5.56}$$

and can be evaluated without knowing the truth finite element solution. For purposes of dual-norm computation we can define the Riesz representant $\widehat{e}(\boldsymbol{\mu})$ s.t.

$$(\widehat{e}(\boldsymbol{\mu}), (\widetilde{\boldsymbol{v}}_h, \widetilde{q}_h))_X = \mathcal{R}_{\boldsymbol{\mu}}(\widetilde{\boldsymbol{v}}_h, q_h) \quad \text{for all } (\widetilde{\boldsymbol{v}}_h, \widetilde{q}_h) \in X_h \tag{5.57}$$

for which $||\widehat{e}(\boldsymbol{\mu})||_X = ||\mathcal{R}_{\boldsymbol{\mu}}(\,\cdot\,,\,\cdot\,)||_{X_h'}$. By applying the Babuška stability result (5.47) and the inf-sup constant (5.46), we have

$$\varphi(\boldsymbol{\mu}) \, ||(\boldsymbol{e}_u, e_p)||_X \leq \sup_{\widetilde{\boldsymbol{v}} \in \mathcal{V}, \widetilde{q} \in \widetilde{\mathcal{Q}}} \frac{\mathcal{A}(\boldsymbol{e}_u, \widetilde{\boldsymbol{v}}; \boldsymbol{\mu}) + \mathcal{B}(e_p, \widetilde{\boldsymbol{v}}; \boldsymbol{\mu}) + \mathcal{B}(\widetilde{q}, \boldsymbol{e}_u; \boldsymbol{\mu})}{||(\widetilde{\boldsymbol{v}}, \widetilde{q})||_X}$$
$$= ||\mathcal{R}_{\boldsymbol{\mu}}(\,\cdot\,,\,\cdot\,)||_{X_h'} = ||\,\widehat{e}(\boldsymbol{\mu})\,||_X. \tag{5.58}$$

Thus for any computable lower bound $\varphi_{\mathrm{LB}}(\boldsymbol{\mu})$ for the parametric stability factor s.t. $0 < \varphi_{\mathrm{LB}}(\boldsymbol{\mu}) \leq \varphi(\boldsymbol{\mu})$ for all $\boldsymbol{\mu} \in \mathcal{D}$, the error estimator

$$\Delta_N(\boldsymbol{\mu}) := \frac{||\,\widehat{e}(\boldsymbol{\mu})\,||_X}{\varphi_{\mathrm{LB}}(\boldsymbol{\mu})} \tag{5.59}$$

gives an upper bound for the error $||(\boldsymbol{e}_u, e_p)||_X$.

5.5 Estimation of the parametric stability factor

The difficulty related to the estimator (5.59) is that the definition of the parametric Babuška inf-sup involves the combination of two different bilinear forms $\mathcal{A}$ and $\mathcal{B}$ that, to our knowledge, has not been as widely analyzed as the Babuška-Brezzi inf-sup constant, which involves only $\mathcal{B}$. A successive constraint method (SCM) [23] for the construction of a lower bound $\varphi_{\mathrm{LB}}(\boldsymbol{\mu}) > 0$ for the inf-sup constant was given in [21] and it works in practice also in the Stokes case. We present briefly an outline of that work with emphasis on our Stokes application (the noncoercive problem treated in the original paper was the Helmholtz equation).

First define the Babuška supremizer operator $\mathbb{T}^{\boldsymbol{\mu}} : X \to X$ as the solution of

$$(\mathbb{T}^{\boldsymbol{\mu}}U, V)_X = \Phi(U, V; \boldsymbol{\mu}) \quad \text{for all } V \in X. \tag{5.60}$$

Note that this operator acts on the whole Stokes system whereas the supremizer operator $T^{\boldsymbol{\mu}}$ acts only on the pressure. Similarly to the other supremizer operator it holds that, due to (5.60), we have

$$\sup_{V \in X} \frac{\Phi(U, V; \boldsymbol{\mu})}{||U||_X ||V||_X} = \frac{\Phi(U, \mathbb{T}^{\boldsymbol{\mu}}U; \boldsymbol{\mu})}{||U||_X ||\mathbb{T}^{\boldsymbol{\mu}}U||_X} = \frac{||\mathbb{T}^{\boldsymbol{\mu}}U||_X}{||U||_X}. \tag{5.61}$$

Note that the evaluation of $\varphi(\boldsymbol{\mu})$ at a given point can be performed by observing that in the discrete case

$$\varphi_h^2(\boldsymbol{\mu}) = \left[\inf_{U_h \in X_h} \sup_{V_h \in X_h} \frac{\Phi(U_h, V_h; \boldsymbol{\mu})}{||U_h||_X ||V||_X} \right]^2 = \left[\inf_{U_h \in X_h} \frac{||\mathbb{T}^{\boldsymbol{\mu}} U_h||_X}{||U_h||_X} \right]^2 = \inf_{U_h \in X_h} \frac{||\mathbb{T}^{\boldsymbol{\mu}} U_h||_X^2}{||U_h||_X^2}$$

$$(5.62)$$

is a problem of finding the least eigenvalue. In matrix form the inner product is defined $(\underline{U}_h, \underline{V}_h)_X = \underline{V}_h^t \underline{X} \underline{U}_h$ using a s.p.d. matrix $\underline{X}$ with Cholesky decomposition $\underline{X} = \underline{H}^t \underline{H}$ and thus after some computations we obtain the following matrix eigenvalue problem: find the smallest $\varphi_h^2(\boldsymbol{\mu})$ s.t.

$$\left[\underline{H}^{-t} \underline{\Phi}(\boldsymbol{\mu}) \underline{X} \ \underline{\Phi}(\boldsymbol{\mu}) \underline{H}^{-1} \right] \underline{V}_h = \varphi_h^2(\boldsymbol{\mu}) \underline{V}_h \quad \text{for some } \underline{V}_h \neq 0. \quad (5.63)$$

The SCM was originally proposed for computing a parametric lower bound for the least eigenvalue of coercive problems that could be affinely decomposed into Q terms with complexity that is linear in Q (but depends explicitly on $\mathcal{N}$ and thus rather expensive). While the same could be done to find a parametric lower bound for (5.63), the operator has Q^2 affine terms and the standard approach is much too cumbersome for problems with larger Q. A modification of the SCM is thus needed for noncoercive problems.

The *local natural norm* version of SCM for noncoercive problems seeks a lower bound for a surrogate inf-sup constant that, for a fixed parameter value $\bar{\boldsymbol{\mu}}$, is defined as

$$\bar{\varphi}_{\bar{\boldsymbol{\mu}}}(\boldsymbol{\mu}) = \inf_{U \in X} \frac{\Phi(U, \mathbb{T}^{\bar{\boldsymbol{\mu}}} U; \boldsymbol{\mu})}{||\mathbb{T}^{\bar{\boldsymbol{\mu}}} U||_X^2}. \quad (5.64)$$

Values of $\bar{\varphi}_{\bar{\boldsymbol{\mu}}}(\boldsymbol{\mu})$ are solutions of the eigenproblem (in matrix form) to find the smallest $\bar{\varphi}_{\bar{\boldsymbol{\mu}}}(\boldsymbol{\mu})$ s.t.

$$\left[\underline{H} \ \underline{\Phi}(\boldsymbol{\mu}) \underline{\Phi}^{-1}(\bar{\boldsymbol{\mu}}) \underline{H}^{-1} \right] \underline{V}_h = \bar{\varphi}_{\bar{\boldsymbol{\mu}}}(\boldsymbol{\mu}) \underline{V}_h \quad \text{for some } \underline{V}_h \neq 0. \quad (5.65)$$

Unlike the version (5.63), for $\bar{\boldsymbol{\mu}}$ fixed the operator contains only Q affine terms. In some neighborhood $\mathcal{P}_{\bar{\boldsymbol{\mu}}} \ni \bar{\boldsymbol{\mu}}$ it holds that $||\mathbb{T}^{\bar{\boldsymbol{\mu}}} U||_X \geq C ||U||_X$ for all $U \in X$, and thus the $|| \cdot ||_X$ norm and the natural norm $||\mathbb{T}^{\bar{\boldsymbol{\mu}}} \cdot ||_X$ are equivalent in that neighborhood. It can be shown that $\varphi(\bar{\boldsymbol{\mu}}) \bar{\varphi}_{\bar{\boldsymbol{\mu}}}(\boldsymbol{\mu}) \leq \varphi(\boldsymbol{\mu})$ and therefore it suffices to seek a lower bound for the surrogate (5.64). This surrogate problem is coercive, so the standard successive constraint method [23] can be used. Through an iterative greedy procedure it finds a set of constraint points around which we define a set of linear constraints to find a positive lower bound for $\bar{\varphi}_{\bar{\boldsymbol{\mu}}}(\boldsymbol{\mu})$ in the entire neighborhood $\mathcal{P}_{\bar{\boldsymbol{\mu}}}$. When this is performed for sufficiently many $\bar{\boldsymbol{\mu}}$ the sets $\mathcal{P}_{\bar{\boldsymbol{\mu}}}$ cover the entire parameter range and we can compute a parametric lower bound for $\varphi(\boldsymbol{\mu})$ accordingly. For details of the local lower bound construction for $\bar{\varphi}_{\bar{\boldsymbol{\mu}}}(\boldsymbol{\mu})$ in $\mathcal{P}_{\bar{\boldsymbol{\mu}}}$, we refer to [21].
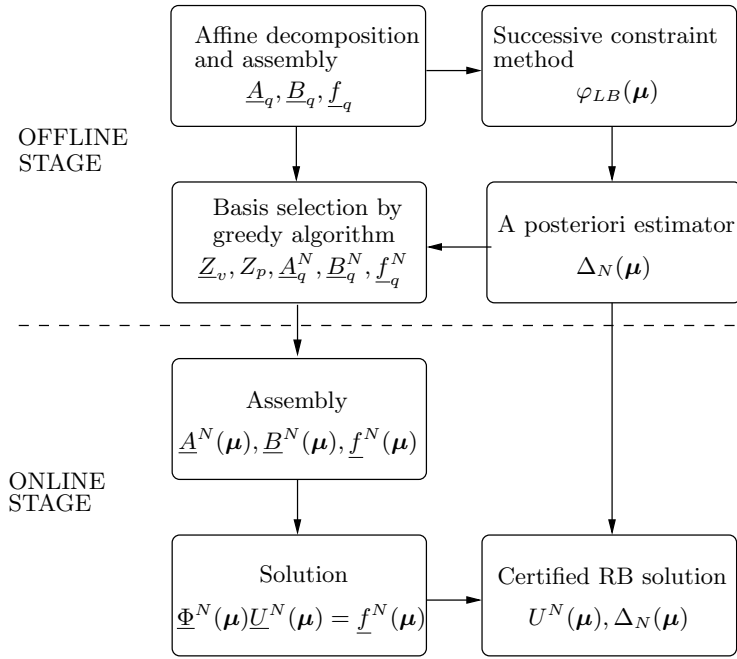
Figure 3: Schematic description of the offline and online stages of the RB method. All the structures created in the offline stage are independent of $\boldsymbol{\mu}$, and thus are computed once and stored in preparation for the online stage. The online stage is independent of the truth FEM dimension $\mathcal{N}$ once these structures have been precomputed.

5.6 An offline/online procedure for the reduced basis method

In Fig. 3 we give a general outline of the reduced basis offline and online stages. The affine decomposition of the parametrized problem matrices and right-hand sides (5.36) allows the assembly and storage of the necessary structures as the first step of the offline stage. Using these structures the successive constraint method can then be used to derive a lower bound manifold for the inf-sup constant $\varphi(\boldsymbol{\mu})$. This involves the solution of $\mathcal{O}(\widehat{Q})$ initial eigenproblems as well as the solution of several linear programming problems of size $\widehat{Q}$ with $\mathcal{O}(\widehat{Q})$ constraints. Thus the complexity of SCM is not only dependent on $\mathcal{N}$, but also magnified by a factor relating to the inherent complexity of the parametrization as codified by the number of affine terms $\widehat{Q}$. As is typical for offline-online reduction schemes, the cost of the offline stage is therefore orders of magnitude larger than the cost of one finite element solution of the parametric PDE.

Once the inf-sup lower bound has been constructed, the estimator (5.59) is used to drive a greedy algorithm [20], such as the one detailed in Algorithm 5.1. The algorithm selects hierarchically the velocity and pressure basis functions according to the at each iteration worst approximated element of a training set, computes the supremizer (5.53) and adds it to the velocity basis, and performs an orthonormalization to improve the algebraic conditioning of the . Finally, the reduced order matrices and right-hand sides (5.39) are computed and stored. With the assumption of affine parameter dependence, the computation of the residual (5.57) in the a posteriori estimator can be treated with a similar offline-online procedure. In matrix form we can write the vectors $\underline{U}_h^N(\boldsymbol{\mu})$ and $\underline{V}_h^N(\boldsymbol{\mu})$ in the reduced basis expansion

$$\underline{U}_h^N(\boldsymbol{\mu}) = \sum_{n=1}^{N} U_n^N(\boldsymbol{\mu})\underline{\zeta}_U^n, \quad \underline{V}_h^N(\boldsymbol{\mu}) = \sum_{n=1}^{N} V_n^N(\boldsymbol{\mu})\underline{\zeta}_U^n \qquad (5.66)$$

so that the residual can be affinely decomposed

$$\begin{aligned} R(V; \boldsymbol{\mu}) &= \sum_{q=1}^{Q_f} \Theta_q^f(\boldsymbol{\mu})F_q(V) - \sum_{q=1}^{Q} \Theta_q^\Phi(\boldsymbol{\mu})\Phi_q(U_h^N, V) \\ &= \sum_{q=1}^{Q_f} \Theta_q^f(\boldsymbol{\mu})F_q(V) - \sum_{n=1}^{N} u_n^N(\boldsymbol{\mu})\sum_{q=1}^{Q} \Theta_q^\Phi(\boldsymbol{\mu})\Phi_q(\zeta_U^n, V) \end{aligned}, \qquad (5.67)$$

which together with (5.57) implies

$$\widehat{e}(\boldsymbol{\mu}) = \sum_{q=1}^{Q_f} \Theta_q^f(\boldsymbol{\mu})C_q - \sum_{n=1}^{N} u_n^N(\boldsymbol{\mu})\sum_{q=1}^{Q} \Theta_q^\Phi(\boldsymbol{\mu})L_q^n \qquad (5.68)$$

23

where $(C_q, V)_X = F_q(V)$ for all $V \in X^h$ and $(L_q^N, V)_X = \Phi(\zeta_U^n, V)$ for all $V \in X^h$. Then

$$||\widehat{e}(\boldsymbol{\mu})||_X^2$$

$$= \sum_{q=1}^{Q_f} \sum_{q'=1}^{Q_f} \Theta_q^f(\boldsymbol{\mu})\Theta_{q'}^f(\boldsymbol{\mu})(C_q, C_{q'})_X$$

$$- \sum_{q=1}^{Q} \sum_{n=1}^{N} u_n^N(\boldsymbol{\mu})\Theta_q^\Phi(\boldsymbol{\mu}) \left[2\sum_{q=1}^{Q_f} \Theta_q^f(\boldsymbol{\mu})(C_q, L_q^n)_X - \sum_{q'=1}^{Q} \sum_{n'=1}^{N} u_{n'}^N(\boldsymbol{\mu})\Theta_{q'}^\Phi(\boldsymbol{\mu})(L_q^n, L_{q'}^{n'})_X \right]$$

(5.69)

The inner products $(C_q, C_{q'})_X$, $(C_q, L_q^n)_X$, $(L_q^n, L_{q'}^{n'})_X$ can be precomputed at the end of the offline stage and stored in the offline stage once the reduced basis $\{\zeta_U^n\}_{n=1}^N$ has been selected. In the online stage the norm of the residual can then be evaluated from the formula (5.69) for each $\boldsymbol{\mu}$ with complexity only involving N.

Algorithm 5.1 Greedy reduced basis selection

Require: Large training sample $\Xi_{\text{train}}^{\text{RB}} \subset \mathcal{P}$, initial snapshot parameter value $\boldsymbol{\mu}^1$

1: Let $n = 1$.
2: Set the first reduced basis vectors $\zeta_v^1 = \frac{\widetilde{\boldsymbol{u}}_h(\boldsymbol{\mu}^1)}{||\widetilde{\boldsymbol{u}}_h(\boldsymbol{\mu}^1)||_{\widetilde{\mathcal{V}}}}$, and $\zeta_p^1 = \frac{\widetilde{p}_h(\boldsymbol{\mu}^1)}{||\widetilde{p}_h(\boldsymbol{\mu}^1)||_{\widetilde{\mathcal{Q}}}}$
3: **repeat**
4:     Compute $(C_q, L_q^n)_X$ and $(L_q^n, L_{q'}^{n'})_X$ for $n' = 1, \ldots, n$ and $q = 1, \ldots, Q$ needed to evaluate $\Delta_n(\boldsymbol{\mu})$ via (5.69).
5:     Choose next parameter using the estimator $\boldsymbol{\mu}^{n+1} = \text{argmax}_{\boldsymbol{\mu} \in \Xi_{\text{train}}^{\text{RB}}} \Delta_n(\boldsymbol{\mu}^{n+1})$. and compute the corresponding snapshot FE solution $(\widetilde{\boldsymbol{u}}_h(\boldsymbol{\mu}^{n+1}), \widetilde{p}_h(\boldsymbol{\mu}^{n+1}))$.
6:     Compute the next supremizer by solving $\underline{X}s(\boldsymbol{\mu}^{n+1}) = \underline{B}(\boldsymbol{\mu}^{n+1})\underline{\widetilde{p}}_h(\boldsymbol{\mu}^{n+1})$.
7:     Orthonormalize to get the next basis vectors and supremizers

$$z_v^{n+1} = \widetilde{\boldsymbol{u}}_h(\boldsymbol{\mu}^{n+1}) - \sum_{n'=1}^{n} \zeta_v^{n'}(\widetilde{\boldsymbol{u}}_h(\boldsymbol{\mu}^{n+1}), \zeta_v^{n'})_{\widetilde{\mathcal{V}}}$$

$$z_p^{n+1} = \widetilde{p}_h(\boldsymbol{\mu}^{n+1}) - \sum_{n'=1}^{n} \zeta_p^{n'}(\widetilde{p}_h(\boldsymbol{\mu}^{n+1}), \zeta_p^{n'})_{\widetilde{\mathcal{Q}}}$$

$$\zeta_v^{n+1} = \frac{z_v^{n+1}}{||z_v^{n+1}||_{\widetilde{\mathcal{V}}}}, \quad \zeta_s^{n+1} = \frac{s^{n+1}}{||s^{n+1}||_{\widetilde{\mathcal{V}}}},$$

8: **until** $\Delta_n(\boldsymbol{\mu}^{n+1}) \leq \text{TOL}$

---

6 Numerical results

To demonstrate the reliability of the RB method for the parametrized Stokes equations, we used a simplified FFD parametrization with $P = 2$ parameters. The reference domain $\Omega = (0,3) \times (-1,0)$ represents a half-width of the actual channel owing to symmetry, and its radius was taken as $R_0 = 0.5$ cm. The free-form deformation used a 4×2 regular grid of control points, where only the 2 central points on the upper row were allowed to move freely in the x_2-direction. In Fig. 4(a) we present the resulting deformed image of the reference domain in two different parameter configurations overlaid with the corresponding positions of the control points. For the Stokes problem using $\mathbb{P}_2/\mathbb{P}_1$-elements this mesh gives a total of $\mathcal{N}_f = 7940$ degrees of freedom. We choose to refine locally the mesh near the free boundary Γ_w and the outlet Γ_{out}, since in our experience these parts yield the largest contribution to the error in the reduced basis approximation of the Stokes equations. The viscosity was chosen as the physiological value $\nu = 0.035$ g/cm·s, and the parabolic inflow velocity $\boldsymbol{g}(x_2) = \begin{bmatrix} 30(1 - (1 + x_2)^2) & 0 \end{bmatrix}^t$ cm/s.

(a)

(b)
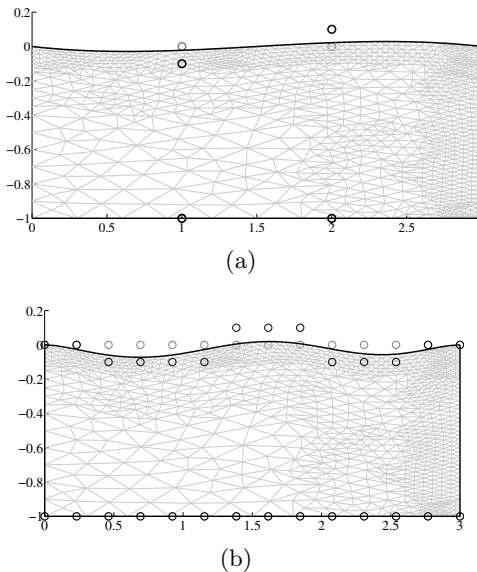
Figure 4: Two different parametric configurations of $\Omega_o(\boldsymbol{\mu})$ induced by the FFD in case (a) $P = 2$ and (b) $P = 10$. Positions of control points in the reference and deformed configurations marked in by $\circ$.

The transformation tensors (3.11) and (3.12) were computed symbolically using a Computer Algebra System (CAS). The empirical interpolation procedure was used to obtain an affinely parametrized version of the Stokes equations on the reference domain. The transformation tensor elements were evaluted by the CAS and the EIM procedure was used to obtain an affine ap-
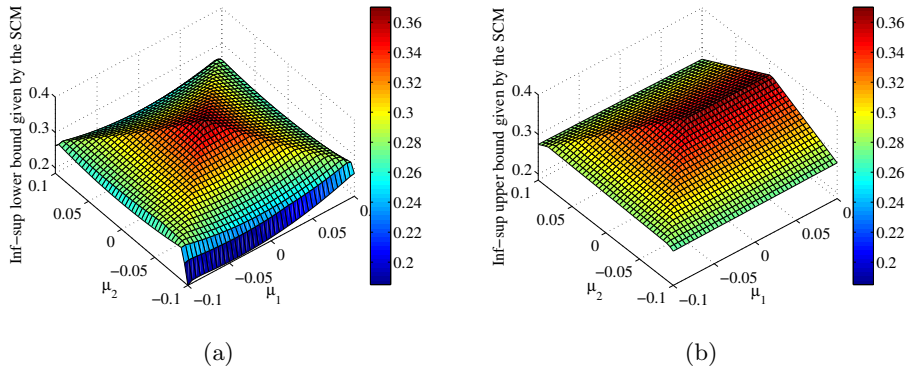
Figure 5: Successive constraint method obtained (a) lower bound surface $\varphi_{\mathrm{LB}}(\boldsymbol{\mu})$ and (b) upper bound surface $\varphi_{\mathrm{UB}}(\boldsymbol{\mu})$ for the parameter-dependent Babuska inf-sup constant

proximate expansion for each tensor component separately. With a stopping tolerance of 1e-5 in the L^∞-norm the total number of terms was $Q_a = 31$ for the viscous part the and $Q_b = 7$ for the (affine) pressure-divergence part. The pressure-divergence tensor being affinely parametrized it would also be possible to derive by hand the affine decompositions, nevertheless, to be consistent in treating the different coefficient functions we used the empirical interpolation method on both parts. When the EIM is applied to an affinely parametrized function it simply stops after a finite number of steps as the error drops to zero (up to machine precision).

6.1 Reduction of the parametric Stokes problem with $P = 2$

After the flow channel has been parametrized with FFDs and the affinely parametric decomposition of the problem has been achieved using the EIM, we can apply the reduced basis machinery. Using the same parameter range as for the EIM, $\mu_1, \mu_2 \in [-0.1, 0.1]$, we used the SCM to compute a lower bound for the parametric Babuska inf-sup constant $\varphi_{\mathrm{LB}}(\boldsymbol{\mu})$. It turns out that for this parametrization the SCM only needed one $\bar{\boldsymbol{\mu}} = [0, 0]$, plus 6 constraint points $\boldsymbol{\mu}_{\bar{\boldsymbol{\mu}}}^j$ in $\mathcal{C}_{\bar{\boldsymbol{\mu}}}$ to achieve 100% coverage of the entire training sample up to the acceptable tolerance for the bound gap, i.e.

$$\frac{\varphi_{\mathrm{UB}}(\boldsymbol{\mu}) - \varphi_{\mathrm{LB}}(\boldsymbol{\mu})}{\varphi_{\mathrm{UB}}(\boldsymbol{\mu})} \leq 0.25 \quad \text{for all } \boldsymbol{\mu} \in \Xi_{\mathrm{train}}^{\mathrm{SCM}}. \tag{6.70}$$

In Fig. 5 we present the online lower bound estimate $\varphi_{\mathrm{LB}}(\boldsymbol{\mu})$ and upper bound estimate $\varphi_{\mathrm{UB}}(\boldsymbol{\mu})$ computed for the entire parameter range. The lower bound is everywhere positive, and therefore the SCM can be deemed to have been successful.

Using the a posteriori estimate (5.59) and the greedy Algorithm 5.1 for basis selection, a total of $N_{\max} = 10$ basis functions were chosen to satisfy the tolerance $\Delta_N(\boldsymbol{\mu}) < $ 1e-5 for all $\boldsymbol{\mu} \in \Xi_{\text{train}}^{\text{RB}}$. After the necessary online structures have been computed, we compare the (affinely decomposed[1]) finite element "truth solution" to the reduced basis approximation using a variable number $N = 1, 2, \ldots, N_{\max}$ of basis functions. In Fig. 6(a) we display the true error and compare it to the a posteriori estimator $\Delta_N(\boldsymbol{\mu})$ for one typical parameter value (in this case $\boldsymbol{\mu} = [0.1, -0.1]$). The convergence is rapid, if not quite exponential, and the gap between the true error and the a posteriori estimator remains more or less the same for all N. In the other plot we show the effectivity of the error estimator

$$\vartheta(\boldsymbol{\mu}) := \frac{\Delta_N(\boldsymbol{\mu})}{||U_h(\boldsymbol{\mu}) - U_h^N(\boldsymbol{\mu})||_X} \tag{6.71}$$

over a random sample of 1000 different parameter points both as an average over the entire sample as well as the best- and worst-case bounds. For a rigorous upper bound we must have $\vartheta \geq 1$ and to have an efficient upper bound we demand that ϑ remains bounded for $N \to \infty$. From Fig. 6 we see that the obtained bounds in this case are both rigorous and efficient.

6.2 Reduction of the parametric Stokes problem with $P = 10$

To test the parametric coupling Algorithm 4.1 we introduced a different FFD parametrization with $P = 10$ parameters. This time we used a 14×2 regular grid of control points, where only the 10 central points on the upper row were allowed to move freely in the x_2-direction. In Fig. 4(b) we present the resulting deformed image of the reference domain in two different parameter configurations overlaid with the corresponding positions of the control points. Again the two left- and rightmost columns of control points were kept fixed. Using a stopping tolerance of 1e-4 in the L^∞-norm for the EIM, the total number of affine terms were $Q_a = 68$ for viscous part the and $Q_b = 22$ for the pressure-divergence part. As we can observe, the number of affine terms grows considerably as a function of the number of FFD parameters P. The acceptable parameter range was again $\mu_p \in [-0.1, 0.1]$ for $p = 1, 2, \ldots, 10$. The discretization of the Stokes problem remained the same.

The natural norm SCM algorithm converges very slowly when the number of parameters is larger than $P \leq 3$. Thus for the setup with $P = 10$ we were not able to obtain a lower bound estimate in a similar fashion. We however observe that for the channel problem adding more free-form parameters does not affect the range of stability factors $\varphi^{-1}(\boldsymbol{\mu})$. In fact, in [55]

---

[1]The nonaffine parametrization strictly speaking adds an extra inconsistency term in the error estimator due to the empirical interpolation error. We forego here the treatment of this small, additional error term, and refer the reader to [34, 48].
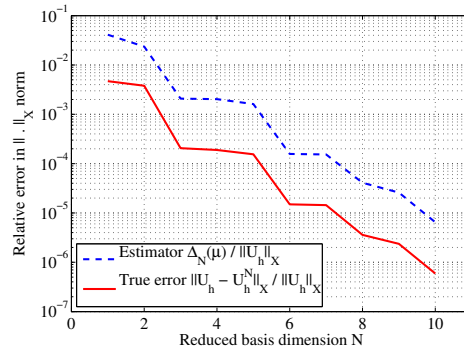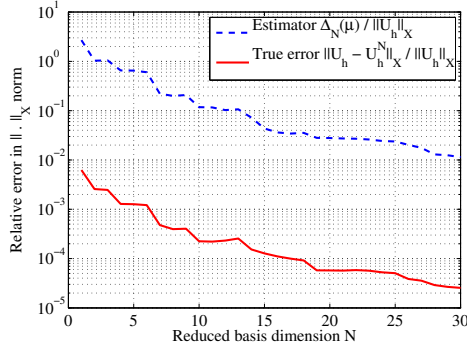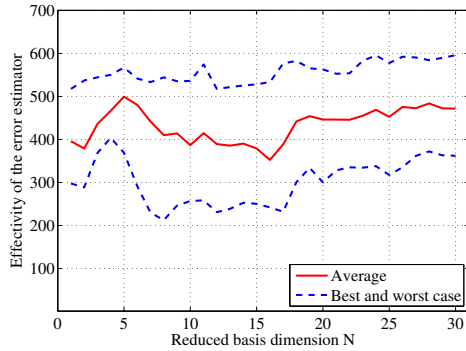
(a)
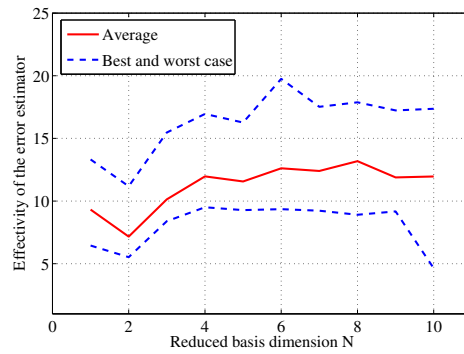
(b)

Figure 6: Case $P = 2$: (a) Relative error between reduced basis solution U_h^n and truth FEM solution U_h and the corresponding error estimate $\Delta_N(\boldsymbol{\mu})$ for one parameter value $\boldsymbol{\mu} \in \mathcal{P}$; (b) Effectivity of the a posteriori error estimator $\Delta_N(\boldsymbol{\mu})$ over a sample set of 1000 different parameter values for different reduced basis dimensions N

(a)

(b)

Figure 7: Case $P = 10$: (a) Relative error between reduced basis solution U_h^n and truth FEM solution U_h and the corresponding error estimate $\Delta_N(\boldsymbol{\mu})$ for one parameter value $\boldsymbol{\mu} \in \mathcal{P}$; (b) Effectivity of the a posteriori error estimator $\Delta_N(\boldsymbol{\mu})$ over a sample set of 1000 different parameter values for different reduced basis dimensions N

it was demonstrated that for a periodic channel the Brezzi inf-sup constant $\beta(\boldsymbol{\mu})$ (which is related to the Babuška inf-sup constant, see e.g. [46]) depends mostly on the width of the narrowest part of the channel. Thus we circumvented the problems related to the SCM by using a global constant, $\varphi_{\mathrm{LB}} = 0.185$ for all $\boldsymbol{\mu} \in \mathcal{D}$, as the lower bound. This was obtained according to Fig. 5(a) from the case $P = 2$. The greedy Algorithm 5.1 for basis selection was driven to select a fixed number of $N_{\max} = 30$ basis functions. In Fig. 7 we show as before the error estimate and its effectivity over a random sample of 1000 different parameter points. Despite the rather pessimistic bound for the parametric stability factor the resulting estimator still has reasonable effectivity. The relative error of the reduced Stokes solutions is slightly larger than in the previous case, but still less than 0.1%.

29

6.3 Convergence and accuracy of the coupling algorithm

To test the parametric coupling algorithm the structural equations were discretized with 1-d cubic Hermite elements using $\mathcal{N}_s = 82$ degrees of freedom. In this case it was not necessary to apply a further reduction to the structural equations, which were always solved using the full finite element model. The physical parameters of the structural equations were chosen as $E = 0.75 \cdot 10^6$ dyn/cm^2, $h = 0.1$ cm, $\nu_P = 0.5$, $K = 0.9643$, and $G = 0.20 \cdot 10^6$ dyn/cm^2 according to [11]. The fourth order perturbation term was chosen according to two different values, $\varepsilon = $ 1e-2 and $\varepsilon = $ 1e-3. In the former case the shape of the deformed tube is closer to being symmetric, while in the latter case we obtain a highly unsymmetric deformed shape due to the reduced stiffness of the wall and the pressure profile imposed by the mixed boundary conditions. In Fig. 8 we display a visualization of the displacement of the structure at the end of the coupling iteration in both of the aforementioned cases.

(a)

(b)
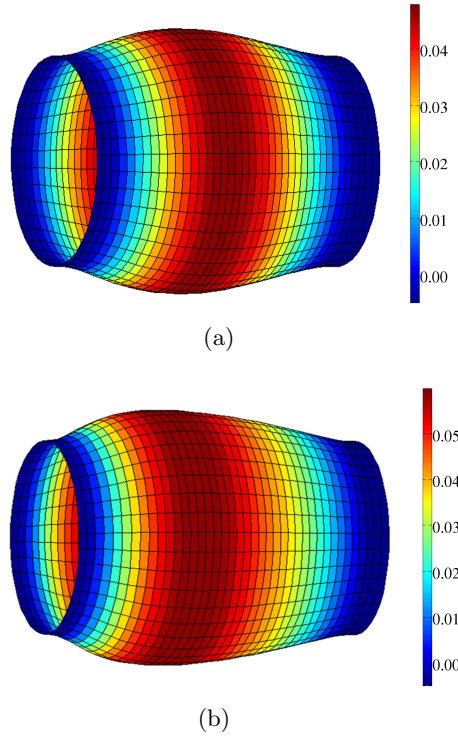
Figure 8: Visualization of the displacement of the structure of the coupled solution (displacements magnified) for (a) $\varepsilon = $ 1e-2 and (b) $\varepsilon = $ 1e-3.

For $P = 10$ parameters and $\varepsilon = $1e-2 the fixed point algorithm converged in 6 major iterations (reduced fluid + structure solutions) to a tolerance of $|\boldsymbol{\mu}^k - \boldsymbol{\mu}^{k-1}| < $ 1e-6. The numbers of optimization iterations (without PDE solutions) for the NLP solver at each iteration were (74, 56, 20, 11, 2, 1),

where the optimization problem was solved at each iteration to a relative stopping tolerance of 1e-6. We use the relative error of the L^2-norm between the assumed displacement and the structural displacement to measure the coupling accuracy. In this case after the final iteration we obtained

$$\frac{||\eta(\boldsymbol{\mu}^k) - \widehat{\eta}(\boldsymbol{\mu}^k)||}{||\eta(\boldsymbol{\mu}^k)||} = 1.112\text{e-}3 \tag{6.72}$$

The prototype code was written in Matlab and ran serially on one Intel Xeon 2.40 GHz processor with 4 GB of working memory. In this case the coupled solution was obtained in 580 s with the reduced fluid equations, and in 630 s with the full finite element fluid equations. The rather small difference is due to the low number of major iterations (and consequently fluid solutions) required to achieve coupling. In the unsteady case the obtained computational cost savings will be much larger. In any case, the reduced systems of size 30×30 are small enough to be used as part of a very large flow network consisting of hundreds of coupled FSI elements.

To test the coupling accuracy obtained using a different number P' of free-form deformation parameters we defined a monotonically increasing subset of the parameters for $P' = 2, 3, 4, 5, 6, 7, 8, 9$, where the rest of the parameters were fixed at $\mu_p = 0$ in each case. The coupled solution was then computed in each of these cases. In Fig. 9 we display the relative error of the final displacement for different values of P' for $\varepsilon = 1$e-2 and $\varepsilon = 1$e-3, both computed with the reduced fluid equations and the full FEM. The coupling accuracies obtained by using RB and FEM were virtually the same. The theoretical optimal N-width was computed from (4.30). In both cases the coupling accuracy converges at least as fast as the worst-case asymptotic rate predicted by the N-width theory. We read this as an indication that the FFD parametrization is suitable for the problem at hand and allows the user to achieve desired coupling accuracy by selecting the number of FFD parameters P large enough.

7   Conclusions and future work

We have presented a new approach to model reduction of a coupled fluid-structure interaction problem. By introducing a parametric free-form deformation of the flow geometry the fluid equations can be written as parametric partial differential equations on a fixed domain. We then applied the reduced basis method to the fluid equations to obtain an efficient reduced model with certified error bounds. The geometric deformation parameters were also used to couple the fluid domain to a 1-d wall equation, where the parameters acted as the coupling variables. We demonstrated that for a modest number of free-form deformation parameters an approximate coupling between fluid and structure can be achieved. The same coupling accuracy was achieved for both the full finite element fluid model and the
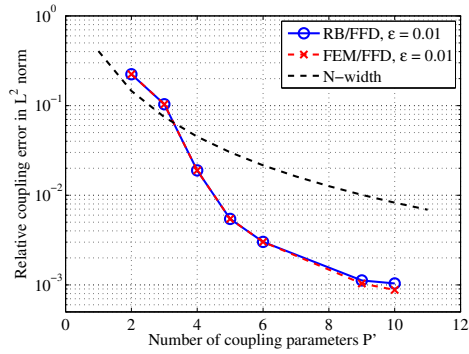
(a)
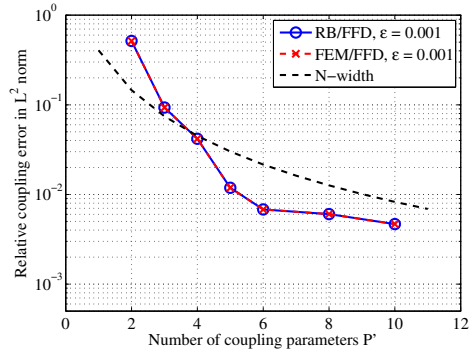
(b)

Figure 9: Relative L^2-error $||\eta - \widehat{\eta}||/||\eta||$ at the end of Algorithm 4.1 for (a) $\varepsilon = 1\text{e-}2$ and (b) $\varepsilon = 1\text{e-}3$. The theoretical N-width is computed according to (4.30).

reduced model with $N = 30$ basis functions. Future work involves extending the approach to the unsteady case and coupling the individual reduced basis fluid-structure models into a large flow network.

Acknowledgements

References

[1] B.O. ALMROTH, P. STERN, AND F.A. BROGAN, *Automatic choice of global shape functions in structural analysis*, AIAA J., 16 (1978), pp. 525–528.

[2] I. BABUŠKA AND A.K. AZIZ, *Lectures on the mathematical foundations of the finite element method*, Tech. Report BN-748, University of Maryland, College Park, Washington DC, 1972.

[3] M. BARRAULT, Y. MADAY, N.C. NGUYEN, AND A.T. PATERA, *An 'empirical interpolation' method: application to efficient reduced-basis discretization of partial differential equations*, C. R. Math. Acad. Sci. Paris, 339 (2004), pp. 667 – 672.

[4] H. BREMER, *Elastic multibody dynamics: a direct Ritz approach*, Springer Science+Business Media, 2008.

[5] C. CANUTO, M.Y. HUSSAINI, A. QUARTERONI, AND TH.A. ZANG, *Spectral Methods: Evolution to Complex Geometries and Applications to Fluid Dynamics*, Springer, 2007.

[6] C. CANUTO, T. TONN, AND K. URBAN, *A posteriori error analysis of the reduced basis method for nonaffine parametrized nonlinear PDEs*, SIAM J. Numer. Anal., 47(3) (2009), pp. 2001–2022.

[7] T. F. COLEMAN AND Y. LI, *An interior trust region approach for nonlinear minimization subject to bounds*, SIAM J. Optimization, 6 (1996), pp. 418–445.

[8] S. Deparis, *Reduced basis error bound computation of parameter-dependent Navier–Stokes equations by the natural norm approach*, SIAM J. Num. Anal., 46 (2008), pp. 2039–2067.

[9] G. Farin, *Curves and surfaces for computer-aided geometric design: a practical guide*, Morgan Kaufmann, 2001.

[10] J.P. Fink and W.C. Rheinboldt, *On the error behavior of the reduced basis technique for nonlinear finite element approximations*, Z. Angew. Math. Mech., 63(1) (1983), pp. 21–28.

[11] L. Formaggia, J.-F. Gerbeau, F. Nobile, and F. Quarteroni, *On the coupling of 3D and 1D Navier-Stokes equations for flow problems in compliant vessels*, Comput. Methods Appl. Mech. Engrg., 191(6-7) (2001), pp. 561–582.

[12] L. Formaggia, A. Quarteroni, and A. Veneziani, *Multiscale models of the vascular system*, In: Formaggia, L.; Quarteroni, A; Veneziani, A. (Eds.), Cardiovascular Mathematics, Springer, (2009).

[13] L. Formaggia, A. Quarteroni, and A. Veneziani (Eds.), *Cardiovascular Mathematics – Modeling and simulation of the circulatory system*, vol. 1 of Modeling, Simulation and Applications, Springer-Verlag Italia, Milano, 2009.

[14] M. Fortin, *Finite element solution of the Navier-Stokes equations*, Acta Numerica, 2 (1993), pp. 239–284.

[15] V. Girault and P.-A. Raviart, *Finite element methods for Navier-Stokes equations: Theory and algorithms*, Springer-Verlag, Berlin and New York, 1986.

[16] R. Glowinski and O. Pironneau, *Toward the computation of minimum drag profile in viscous laminar flow*, Appl. Math. Model., 1 (1976).

[17] C. Grandmont, *Analyse mathématique et numérique de quelques problèmes d'interaction fluide structure*, PhD thesis, Université Paris VI, 1998.

[18] ——, *Existence et unicité de solutions d'un problème de couplage fluide-structure bidimensionnel stationnaire*, C. R. Math. Acad. Sci. Paris, 326 (1998), pp. 651–656.

[19] M.A. Grepl, Y. Maday, N.C. Nguyen, and A.T. Patera, *Efficient reduced-basis treatment of nonaffine and nonlinear partial differential equations*, ESAIM Math. Modelling Numer. Anal., 41(3) (2007), pp. 575–605.

[20] M.A. Grepl and A.T. Patera, *A posteriori error bounds for reduced-basis approximations of parametrized parabolic partial differential equations*, ESAIM Math. Modelling Numer. Anal., 39(1) (2005), pp. 157–181.

[21] D.B.P. Huynh, D. Knezevic, Y. Chen, J. Hesthaven, and A.T. Patera, *A natural-norm successive constraint method for inf-sup lower bounds*, Comput. Methods Appl. Mech. Engrg., 199(29-32) (2010).

[22] D.B.P. Huynh, N.C. Nguyen, A.T. Patera, and G. Rozza, *Rapid reliable solution of the parametrized partial differential equations of continuum mechanics and transport*, 2008. `http://augustine.mit.edu`.

[23] D.B.P Huynh, G. Rozza, S. Sen, and A.T. Patera, *A successive constraint linear optimization method for lower bounds of parametric coercivity and inf-sup stability costants*, C. R. Acad. Sci. Paris. Sér. I Math., 345 (2007), pp. 473–478.

[24] K. Ito and S.S. Ravindran, *A reduced order method for simulation and control of fluid flows*, J. Comp. Phys., 143(2) (1998).

[25] T. Lassila and G. Rozza, *Model reduction of steady fluid-structure interaction problems with free-form deformations and reduced basis methods*, Proc. 10th Finnish Mech. Days, Jyväskylä, Finland, December 2009, (2009), pp. 454–465.

[26] ——, *Parametric free-form shape design with PDE models and reduced basis method*, Comput. Methods Appl. Mech. Engrg., 199(23–24) (2010), pp. 1583–1592.

[27] P. Le Tallec and J. Mouro, *Fluid structure interaction with large structural displacements*, Comput. Methods. Appl. Mech. Engrg., 190 (2001), pp. 3039–3067.

[28] T.W. Lowe and T.J. Pedley, *Computation of Stokes flow in a channel with a collapsible segment*, J. Fluids Struct., 9 (1995), pp. 885–905.

[29] Y. Maday, N.C. Nguyen, A.T. Patera, and G.S.H. Pau, *A general multipurpose interpolation procedure: the magic points*, Commun. Pure Appl. Anal., 8(1) (2009).

[30] Y. Maday, A.T. Patera, and G. Turinici, *Global a priori convergence theory for reduced-basis approximation of single-parameter symmetric coercive elliptic partial differential equations*, C. R. Acad. Sci. Paris. Sér. I Math., 335 (2002), pp. 1–6.

[31] A. Manzoni, A. Quarteroni, and G. Rozza, *Shape optimization for viscous flows by reduced basis methods and free-form deformation*,

Tech. Report 15.2010, MATHICSE, 2010. Online version: `http://cmcs.epfl.ch/publications/techreport`.

[32] T. McInerney and D. Terzopoulos, *Deformable models in medical image analysis: a survey*, Medical Image Anal., 1(2) (1996), pp. 91–108.

[33] C.M. Murea, *The BFGS algorithm for a nonlinear least squares problem arising from blood flow in arteries*, Comput. Math. Appl., 49 (2005), pp. 171–186.

[34] N.C. Nguyen, *A posteriori error estimation and basis adaptivity for reduced-basis approximation of nonaffine-parametrized linear elliptic partial differential equations*, J. Comp. Phys., 227 (2007), pp. 983–1006.

[35] A.K. Noor and J.M. Peters, *Reduced basis technique for nonlinear analysis of structures*, AIAA J., 18(4) (1980), pp. 455–462.

[36] A.T. Patera and G. Rozza, *Reduced Basis Approximation and A Posteriori Error Estimation for Parametrized Partial Differential Equation*, Version 1.0, Copyright MIT 2006, to appear in (tentative rubric) MIT Pappalardo Graduate Monographs in Mechanical Engineering, 2009.

[37] J.S. Peterson, *The reduced basis method for incompressible viscous flow calculations*, SIAM J. Sci. and Stat. Comput., 10(4) (1989), pp. 777–786.

[38] A. Pinkus, *n-Widths in Approximation Theory*, Springer-Verlag, Ergebnisse, 1985.

[39] T.A. Porsching, *Estimation of the error in the reduced basis method solution of nonlinear equations*, Math. Comput., 45(172) (1985), pp. 487–496.

[40] A. Quarteroni and L. Formaggia, *Mathematical modelling and numerical simulation of the cardiovascular system*, In: Ayache, N. (Ed.), Computational Models for the Human Body, Handbook of Numerical Analysis (P.G Ciarlet Ed.), (2004), pp. 3–129.

[41] A. Quarteroni and G. Rozza, *Numerical solution of parametrized Navier-Stokes equations by reduced basis methods*, Numer. Methods Partial Differential Equations, 23(4) (2007), pp. 923–948.

[42] A. Quarteroni, M. Tuveri, and A. Veneziani, *Computational vascular fluid dynamics: problems, models and methods*, Comp. Vis. Sci., 2:163-197 (2000).

[43] A. QUARTERONI AND A. VALLI, *Numerical Approximation of Partial Differential Equations (1st Ed.)*, Springer-Verlag, Berlin-Heidelberg, 1994.

[44] ——, *Domain Decomposition Methods for Partial Differential Equations*, Oxford University Press, 1999.

[45] G. ROZZA, *Reduced basis methods for Stokes equations in domains with non-affine parameter dependence*, Comput. Vis. Sci., 12(1) (2009), pp. 23–35.

[46] G. ROZZA, D.B.P. HUYNH, AND A. MANZONI, *Reduced basis approximation and a posteriori error estimation for Stokes flows in parametrized geometries: roles of the inf-sup stability constants*, Tech. Report 22.2010, MATHICSE, 2010. Online version: `http://cmcs.epfl.ch/publications/techreport`.

[47] G. ROZZA, D.B.P. HUYNH, AND A.T. PATERA, *Reduced basis approximation and a posteriori error estimation for affinely parametrized elliptic coercive partial differential equations*, Arch. Comput. Methods Engrg., 15 (2008), pp. 229–275.

[48] G. ROZZA, T. LASSILA, AND A. MANZONI, *Reduced basis method for shape optimization in thermal flows parameterized with a polynomial geometric map*, In: Einar Rønquist, Jan S. Hesthaven (Eds.) Proceedings of International Conference on Spectral and High-Order Methods, Trondheim, Norway. Lecture Notes in Computational Science and Engineering, Springer, (2010).

[49] G. ROZZA AND A. MANZONI, *Model order reduction by geometrical parametrization for shape optimization in computational fluid dynamics*, In: J. C. F. Pereira and A. Sequeira (Eds.) Proc. V European Conf. Computat. Fluid Dynamics, ECCOMAS CFD 2010, Lisbon, Portugal, 14–17 June, (2010).

[50] G. ROZZA AND K. VEROY, *On the stability of Reduced Basis methods for Stokes Equations in parametrized domains*, Comput. Methods Appl. Mech. Engrg., 196 (2007), pp. 1244–1260.

[51] J.A. SAMAREH, *Survey of shape parameterization technique for high-fidelity multidisciplinary shape optimisation*, AIAA J., 39(5) (2001), pp. 877–884.

[52] T.W. SEDERBERG AND S.R. PARRY, *Free-form deformation of solid geometric models*, Comput. Graph., 20(4) (1986).

[53] K.G. VAN DER ZEE, E.H. VAN BRUMMELEN, AND R. DE BORST, *Goal-oriented error estimation for Stokes flow interacting with a flexible channel*, Int. J. Numer. Meth. Fluids, 56 (2008), pp. 1551–1557.

[54] K. VEROY AND A.T. PATERA, *Certified real-time solution of the parametrized steady incompressible Navier-Stokes equations: rigorous reduced-basis a posteriori error bounds*, Int. J. Numer. Meth. Fluids, 47(8-9) (2005), pp. 773–788.

[55] J. WILKENING, *Inf-sup estimates for the Stokes problem in a periodic channel*, arXiv.org, [math.AP] 0706.4082v1 (2007).

10.2010   J. BONNEMAIN :
From medical images to numerical simulations

11.2010   G. ROZZA :
Reduced basis approximation and error bounds for potential flows in parametrized geometries

12.2010   F. GELSOMINO, G. ROZZA :
Comparison and combination of reduced order modelling techniques in 3D parametrized heat transfer problems

13.2010   T. LASSILA, G. ROZZA:
Reduced formulation of a steady-fluid structure interaction problem with parametric coupling

14.2010   P. BLANCO, M. DISCACCIATI, A. QUARTERONI :
Modeling dimensionally-heterogeneous problems: analysis, approximation and applications

15.2010   A. MANZONI, A. QUARTERONI, G. ROZZA:
Shape optimization for viscous flows by reduced basis methods and free-form deformation

16.2010   M. J. GROTE, I. SIM:
Local nonreflecting boundary condition for time-dependent multiple scattering

17.2010   A. C. I. MALOSSI, P. J BLANCO, S. DEPARIS, A. QUARTERONI:
Algorithms for the partitioned solution of weakly coupled fluid models for cardiovascular flows

18.2010   M. DISCACCIATI, A. QUARTERONI, S. QUINODOZ:
Numerical approximation of internal discontinuity interface problems

19.2010   B. KALTENBACHER, M. KALTENBACHER, I. SIM:
Perfectly matched layer technique for the second order wave equations in time domain

20.2010   T. LASSILA, G. ROZZA:
Model reduction of semiaffinely parameterized partial differential equations by two-level affine approximation

21.2010   T. HOFER, J. RAPPAZ:
Numerical conservation schemes for convection-diffusion equations

22.2010   G. ROZZA, D.B. PHUONG HUYNH, A. MANZONI :
Reduced basis approximation and a posteriori error estimation for Stokes flows in parametrized geometries : roles of the inf-sup stability constants

01.2011   T. LASSILA, A. QUARTERONI, G. ROZZA :
A reduced basis model with parametric coupling for fluid-structure interaction problems